VHF-UHF Measurements of Lightning

by

Rahulkumar Solanki

Department of Electrical and Computer Engineering
Duke University

Date:_____
Approved:

_____
Steven Cummer, Supervisor

_____
Ronen Plesser

_____
Thomas Katsouleas

Thesis submitted in partial fulfillment of
the requirements for the degree of
Master of Science in the Department of
Electrical and Computer Engineering in the Graduate School
of Duke University

2012

ABSTRACT

VHF-UHF Measurements of Lightning

by

Rahulkumar Solanki

Department of Electrical and Computer Engineering
Duke University

Date:_____
Approved:

_____
Steven Cummer, Supervisor

_____
Ronen Plesser

_____
Thomas Katsouleas

An abstract of a thesis submitted in partial
fulfillment of the requirements for the degree
of Master of Science in the Department of
Electrical and Computer Engineering in the Graduate School of
Duke University

2012

Copyright by
Rahulkumar Solanki
2012

# Abstract

Universal software radio peripheral (USRP) was utilized to receive the radiation produced by lightning flashes in VHF and UHF bands, with the bandwidth ranging from 2MHz to 8MHz. The software radio was programmed to record this radiation by integrating GPS clock and absolute timing. Moreover, two USRP N210 were employed to simultaneously record data at VHF and UHF bands with different programmable gain settings. This data was compared with the data from National Lightning Detection Network (available as location, type and peak current of lightning) and the magnetic sensor operating at LF (30 to 300 kHz). The output of USRP is the antenna displacement current $\frac{\partial E}{\partial t}$ (uncalibrated) and of LF magnetic sensor is the induced voltage $\frac{\partial B}{\partial t}$. From comparison, the following results were obtained. K processes or regular pulse bursts in both cloud and cloud-to-ground flashes were clearly visible at UHF-VHF-LF. These processes were even visible at VHF with 0 dB gain, if superimposed on high magnitude slow (electric field change) processes such as J process probably. Distant narrow bipolar pulses were observed with significant magnitude at VHF. Initial breakdown in cloud discharge was strong at LF and VHF but not significant at UHF. Instead the short pulses, probably stepped leaders, with 1 to 2.5 μs of time duration produced high magnitudes at UHF (while LF pulses remained small yet visible). Moreover, in few cloud discharges some processes occurring during final stage produced strong VHF-UHF radiation.

# Dedication

To my father Jayantilal, my mother Vinodaben and my brother Nehal

# Contents

Abstract ..... iv

List of Tables ..... viii

List of Figures ..... ix

Acknowledgements ..... xiii

1. Introduction to lightning ..... 1

    1.1 Cloud-to-ground flashes ..... 3

    1.2 Cloud flashes ..... 5

2. Introduction to Universal Software Radio Peripheral (USRP) ..... 8

    2.1 As receiver ..... 8

        2.1.1 Quadrature demodulation ..... 9

    2.2 As transmitter ..... 12

        2.2.1 Quadrature modulation ..... 12

    2.3 GPS integration ..... 13

3. Setup ..... 16

4. Measurements with 0 dB gain ..... 19

    4.1 VHF (67-75 MHz) ..... 20

    4.2 UHF (695-715 MHz) ..... 34

5. Measurements at higher gain ..... 38

    5.1 With 8 dB ..... 39

    5.2 With 16 dB ..... 40

6. Useful frequency bands at Duke Campus ..... 42

7. Measurements at Duke Campus ..... 46

7.1 VHF (190-198 MHz) ..... 46

7.2 UHF (608-614 MHz) ..... 48

7.3 Inference of simultaneous UHF-VHF-LF recording ..... 49

References ..... 57

# List of Tables

Table 1: The flashes reported by NLDN, occurred during the time window of Figure 51 ..... 50

# List of Figures

Figure 1: Charge structure of thunder cloud and types of lightning ..... 2

Figure 2: The various processes comprising a negative cloud to ground flash (Rakov and Uman 2003) ..... 3

Figure 3: Block diagram of USRP N210 provided by Ettus research ..... 8

Figure 4: Quadrature sampled signal; only requires half of Nyquist frequency to sample the signal ..... 10

Figure 5: Magnitude of complex baseband is the envelope of the original signal $\mathbf{x}(\mathbf{t})$, just like in amplitude modulation where $\mathbf{x}(\mathbf{t})$ is carrier signal ..... 11

Figure 6: Again magnitude of complex baseband signal as the envelope of the absolute value of signal $\mathbf{x}(\mathbf{t})$ ..... 11

Figure 7: Reconstruction of the original signal, here an offset is added to distinguish two plots which are exactly same ..... 13

Figure 8: On the left, block diagram of internal GPSDO provided by Ettus research, where (A) RS232 (B) 1 PPS (C) 10MHz reference clock (D) Power (E) GPS antenna. On the right, RS232 DB9 pin out (adapted from wiki.robotz.com) ..... 14

Figure 9: Using HyperTerminal to receive the NMEA frames transmitted by internal GPSDO ..... 15

Figure 10: Signal transmitted at 621MHz but the spectrum shows reception at 619MHz as well; spectrum is complex baseband but original frequencies are displayed for convenience ..... 18

Figure 11: Larger marker sizes indicate that the corresponding NLDN lightning flashes are detected in our system (VHF) and vice versa; in the plot, grid lines don't represent constant latitude, longitude circles, instead these circles have same trajectories as in astronomy charts ..... 20

Figure 12: recorded at 73-75 MHZ with 0dB gain (|noise level|< 0.02), NLDN info: event time (first return stroke) 23:39:9.359 (UTC), CG at 12.7175 km with -20kA peak current ..... 21

Figure 13: Corresponding LF plot ..... 21

Figure 14: First return stroke, not producing highest $\boldsymbol{\partial E/\partial t}$ during flash; next pulses may correspond to fine structure (Davis 1999) ..... 22

Figure 15: First return stroke at LF ..... 22

Figure 16: Highest $\boldsymbol{\partial E/\partial t}$ during entire flash ..... 23

Figure 17: Corresponding LF plot; this process cannot be a subsequent return stroke due to the continued small pulses extending beyond the time window of the plot ..... 23

Figure 18: Probably the regular pulse bursts occurring before the highest $\boldsymbol{\partial E/\partial t}$ event . 24

Figure 19: Corresponding LF plot ..... 24

Figure 20: Recorded at 67-69 MHz (|noise level| < 0.02). NLDN info: event time 23:13:8.221 (UTC), IC at 8.5838 km with 12kA peak current ..... 26

Figure 21: corresponding LF plot, no other close lightning flash in the plotted time window ..... 26

Figure 22: K processes with higher magnitude at LF were detected at VHF. This plot shows (recorded at 73-75 MHz) IC at 14.3904 km with 9kA peak current, occurring at 23:38:57.988 ..... 27

Figure 23: Probably the K process superimposed on slower (electric field change) J process producing higher magnitude ..... 27

Figure 24: Closer look at the plot in Figure 3; left most part of circle is at 70 km away from lab in Duke forest, similarly consequent circles to right are 60 and 50 km away respectively. The numbers associated with positive IC are peak currents provided by NLDN ..... 28

Figure 25: Recorded at 67-69 MHz; IC occurring at 23:12:16.193 (UTC) with 9kA current at 70.01 km ..... 29

Figure 26: Corresponding LF plot; no other flash in the plotted time window ..... 29

Figure 27: Zoomed in VHF plot, pulse duration is ~10 μs consistent with (Le Vine 1980) ..... 30

Figure 28: Corresponding LF plot with pulse duration of ~60μs ..... 30

Figure 29: Narrow bipolar event (at 70.64 km with 3kA peak current). ..... 31

Figure 30: Typical IC (with Active and final stage) at distance 55.49 km which wasn't detected at VHF, strongly suggesting the detected IC as narrow bipolar events ..... 32

Figure 31: Probably K process occurring at final stage of the IC in Figure 22..... 32

Figure 32: Maximum of $|\partial \mathbf{E}/\partial \mathbf{t}|$ for positive IC..... 33

Figure 33: Similarly for negative CG ..... 33

Figure 34: Larger marker sizes indicate that the corresponding NLDN lightning flashes were detected in UHF system and vice versa; in the plot, grid lines don't represent constant latitude, longitude circles, instead these circles have same trajectories as in astronomy charts..... 34

Figure 35: Closer look at the plot in Figure 33; left most part of circle is at 20 km away from lab in Duke Forest, similarly next circle at right is 10 km away. The numbers associated with positive IC are peak currents provided by NLDN. ..... 35

Figure 36: Return stroke, undetected at UHF with 0 dB gain and 2 MHz bandwidth (-29 kA peak current and 9.3675km distance for the plotted CG) ..... 35

Figure 37: Similar CG processes in NLDN time window which were undetected at UHF (-29 kA peak current and 9.68 km distance for the plotted CG)..... 36

Figure 38: CG processes inside NLDN time window, detected at UHF. The time duration of such processes were ranging from around 0.003 to 0.06 seconds (-13 kA peak current and 9.83 km distance for the plotted CG)..... 36

Figure 39: UHF (713-715 MHz) activity of the CG ..... 37

Figure 40: Corresponding LF plot..... 37

Figure 41: Each circle with 20 km incremental radius. Events are not displayed that happened during the noisy recordings. No symbol for Negative IC (in legend) means none occurred during the measurements ..... 39

Figure 42: Each circle with 20 km incremental radius; again due to impreciseness of MIMO sync, VHF data wasn't compared with NLDN. Events occurred during noisy recorded data were omitted. ..... 40

Figure 43: Recorded at 71-73 MHZ with 16dB gain. Positive IC not reported by NLDN but should be at close distance (VHF saturated) ..... 41

Figure 44: Corresponding LF plot which is remarkably similar to VHF ..... 41

Figure 45: Recorded at 190-200 MHz, from the spectrograph (195MHz is center frequency shown as 0 in the plot, indicating complex baseband signal), 190-198 MHz is less noisy in frequency domain..... 44

Figure 46: Recorded with 194 MHz center frequency and 7.692308MHz bandwidth, showing less noise in time and frequency domain as expected ..... 45

Figure 47: For negative CG..... 47

Figure 48: For positive IC ..... 47

Figure 49: Maximum of $|\partial \mathbf{E}/\partial \mathbf{t}|$ in 0.1 millisecond time window for negative CG ..... 48

Figure 50: For positive IC ..... 48

Figure 51: From top UHF, VHF and LF plots for flashes in Table 1..... 51

Figure 52: Highest magnitude event at UHF ..... 52

Figure 53: Return stroke most probably..... 53

Figure 54: Regular pulse burst ..... 54

Figure 55: Event of uncertain origin ..... 55

Figure 56: Another event of uncertain origin..... 56

# Acknowledgements

I am more than grateful to Dr. Steven Cummer for giving me the opportunity to work in this area. It started as a summer project and I never anticipated that it will end as a thesis. I also thank him for his advice, suggestions and patience during the research; sometimes nothing went according to the plan and technical problems hindered the progress. Gaopeng Lu worked like a mentor, gave me ride to the Duke Forest many times and gave important suggestions, thanks GP. I am also thankful to Dr. Romit Roy Choudhury for lending the software radio to start with. Bogdan Popa helped numerous times to resolve Linux related issues. I would like to thank Ettus research technical support (Marcus, Josh and Nick) for their prompt responses. Sandeep Agrawal helped me to develop a C program that utilized threads of the CPU for threshold analysis of the recorded data; the program took 3 minutes compared to 3 hours by MATLAB. Finally, I thank my committee members Ronen Plesser and Tom Katsouleas to accept my invitation.

# 1. Introduction to lightning

Above the desert or the ocean, during a normal day, fair weather electric field of 100 V/m exists. The direction of this electric field is downwards, indicating that earth's surface is negatively charged. Our atmosphere is not pure insulator, leakage currents produces fair weather current density of $2\,pA/m^2$ (Feynman, Leighton et al. 1964). Radioactivity from earth's surface generates ions in the air which are responsible for fair weather current. Therefore, the ionization of air should decrease as increase in altitude. However, by using electrometers in high flying balloon the results were quite opposite, the ionization increased with increase in height (The altitudes were far below ionosphere). Cosmic rays are responsible for the ionization (below 50 km) and Franz Hess got Nobel Prize in Physics for this discovery. The potential difference between electrosphere (just above 60 km) and earth's surface is around 300kV. Earth's surface is negatively charged with around $5 \times 10^5\,C$, while equal positive charge is distributed throughout the atmosphere. The whole system can be considered as lossy spherical capacitor with electrosphere as outer shell and earth's surface as inner shell (Rakov and Uman 2003). Now, the fair weather current is around 1 kA ($4\pi {R_{earth}}^2 \times 2\,pAm^{-2} = 4\pi \times (6353 \times 10^3)^2 \times 2 = 1014.37\,A$), which would neutralize the charge in few minutes. Then how the system remains charged? The answer is lightning. Therefore, most of the cloud to ground flashes brings negative charge to the ground. CTR Wilson was the first one to suggest this global circuit, also to use electrostatic measurements to find the

charge structure of thundercloud. The two types of lightning flash are cloud-to-ground and intracloud. The former is referred as CG and the latter as IC. The simplest triple charge structure (with very small negative charge on the top) of lightning producing cloud is shown in the figure below, where on the top is main positive, in the middle is main negative and at the bottom is small positive charge (Williams 1989). Now, according to the atmospheric sign convention, the fair weather electric current, pointing downwards, is taken as positive. Therefore, the IC that is occurring between main negative and positive charge region, where electrons moves upwards to neutralize the positive charge region producing downward current, is taken as positive. This sign convention is opposite of the physics sign conventions, where in spherical coordinate system, the downwards current is taken as negative. Rest of the text will follow the atmospheric sign convention.

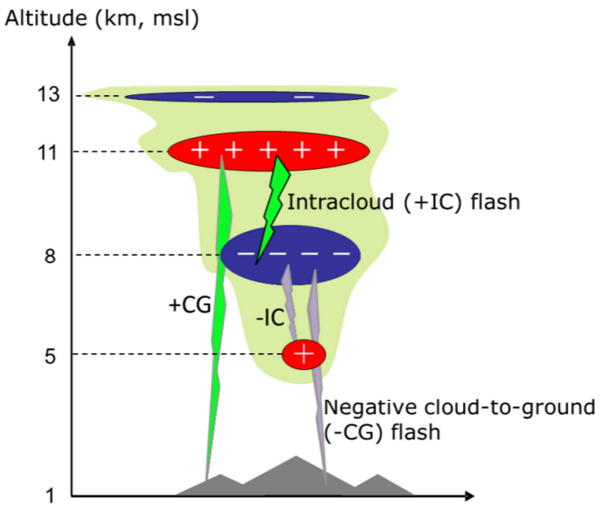


**Figure 1: Charge structure of thunder cloud and types of lightning**

## *1.1 Cloud-to-ground flashes*

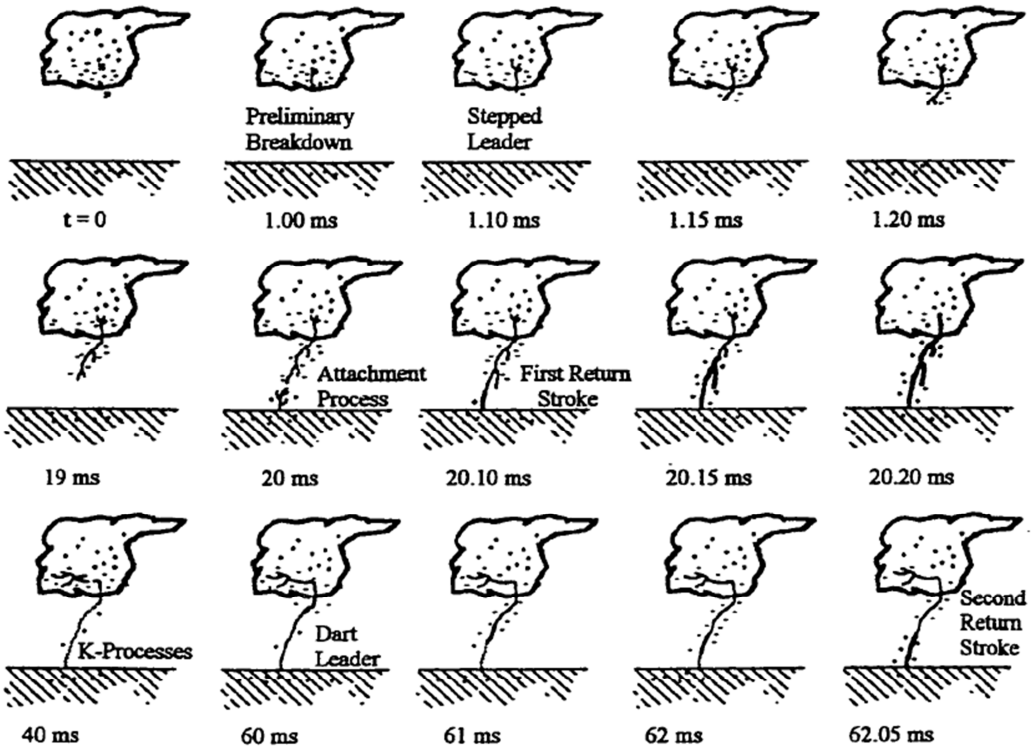


**Figure 2: The various processes comprising a negative cloud-to-ground flash (Rakov and Uman 2003)**

Amongst the four types of the cloud-to-ground flashes, the negative CG (atmospheric sign convention), the one that lowers the negative charge to the ground is the most common. The main negative charge region inside cloud initiates the preliminary breakdown, since the electric field is enormous. The next process is called as stepped leader, which as the name suggests, is the negative charge lowering to the ground in steps and leaving a highly conducting channel behind. The length of each step is around 50 m, the step interval is around 20-50μs and average speed is $2 \times 10^5 m/s$

(Rakov and Uman 2003). The conducting channel is not bright during the stepped leader process. Once the leader is close to ground, the attachment process begins, which is the attachment of positive streamer (due to electrostatic induction) from the ground to the negative leader from cloud. After this process, the highly conducting channel is grounded so the charge neutralization takes place to make the potential difference between cloud and ground zero. The voltage wave that propagates from the ground, neutralizing the entire negatively charged channel is known as return stroke, as the stroke appears to be travelling in the opposite (upward) direction. The propagation speed of return stroke is around half the speed of light. This process is highly luminous (due to recombination of ions) and produces extreme heat which expands the air rapidly and that produces the thunder. After the return stroke, the channel loses the original conductivity with few residual charges left, and temperature decreases so the channel is less bright. Now, after few tens of milliseconds, the second leader comes down following the same path previously taken by stepped leader and travels continuously at around $2 \times 10^7 m/s$ without any steps, which is known as dart leader. Sometimes the leader follows steps, which is known as dart-stepped leader. Again, the second return stroke will neutralize the channel and this leader-stroke process can occur multiple times; Maximum number of return strokes observed in one CG is 26 (Rakov and Uman 2003). J and K processes occur in between two stokes. K processes are thought of the transients occurring during the slower J processes. J processes probably horizontally

transports negative charge to the top of previous stroke (Krehbiel, Brook et al. 1979). K processes lowers the negative charge in the previously conducting channel, although not lowering all the way to ground.

Now, depending upon the leader, the four types of CG are: Negative downward, positive downward, negative upward and positive upward. If the leader is propagating downwards, then the charge of the leader defines the negative or positive downward lightning. Same way, if the leader is propagating upwards from ground (due to tall structures or rocket triggered lightning), then the charge of the leader defines negative or positive upward lightning.

## *1.2 Cloud flashes*

Cloud flashes are of three types: Intracloud, intercloud and cloud to air. These three types of flashes are collectively known as intracloud lightning, abbreviated as IC. Typical IC has two stages: Active stage and final stage (Shao and Krehbiel 1996). The active stage of IC has few similarities with CG, such as initial breakdown and leader moving intermittently, just like stepped leader in CG. However, initial breakdown pulses in IC (50-80μs) are of longer time duration than in CG (20-40μs). The distinction between initial breakdown and stepped leader is still unclear (Rakov and Uman 2003). The final stage processes are smaller in magnitude at VHF-UHF compared to initial stage processes. The final stage consists of transient K processes superimposed on slower (electric field change) J processes. Initial breakdown pulses are slow rising

bipolar with several smaller pulses superimposed on them. Time duration of such pulse is 50-80μs and inter pulse time duration is 600-800μs (Rakov and Uman 2003). K process, also known as regular pulse burst in IC, has inter-pulse duration of 5μs (Davis 1999).

Bilevel flashes connect the main negative charge region to the main positive charge region of the cloud. The model suggests negative leader, originating from main negative charge region, moving intermittently towards main positive charge region and producing single vertical channel. Later in time, negative charges from remote locations are transported to main negative charge region (flash origin) forming predominantly horizontal channels. This negative charge transfer from remote locations is followed by further transfer from origin to upper level. Surprisingly, the return stroke type of process that neutralizes leader channel is absent. Instead, in final stage the cessation of vertical channel occurs. However, negative charges from remote locations may keep transferring to the origin without further transfer to the upper region (due to cessation of vertical channel). Active stage processes significantly changes the electrostatic field inferring the occurrence of charge neutralization. While in final stage, electrostatic field changes are quite small, inferring no charge neutralization. Not all the flashes exhibited final stage.

The other types of IC are bimodal with higher and lower origin lightning. Higher origin IC emits VHF-UHF pulses at much lower rate than lower origin IC, the other differences being step length and interval. The stepped leaders in lower origin IC are

indistinguishable from those in CG. After initial breakdown, predicting the next stage whether CG or IC is difficult (Proctor 1997).

The other two types of IC are predominantly vertical and horizontal lightning. The horizontal flashes (can be both, higher origin or lower origin) consist of predominantly horizontal stepped leader and Q streamers (attributed to K processes) which appear to extend the channel in opposite direction. Q streamers emit light but don't change electrostatic field significantly. According to Mazur (Mahapatra, Doviak et al. 1999), the horizontal flashes start as bidirectional leaders of opposite polarity moving in opposite direction. They postulated that positive leaders don't produce VHF radiation. The recoil streamer originates at the positive leader's tip and travels back and beyond the origin. Predominantly vertical lightning is often thought of inverted cloud to ground flash (Proctor 1981).

# 2. Introduction to Universal Software Radio Peripheral (USRP)

USRP is a portable, high bandwidth software radio system. GNU radio (python) or UHD (universal hardware driver, C++ API) can be used to program such radio. To better understand the hardware, let's start with the receiving part.

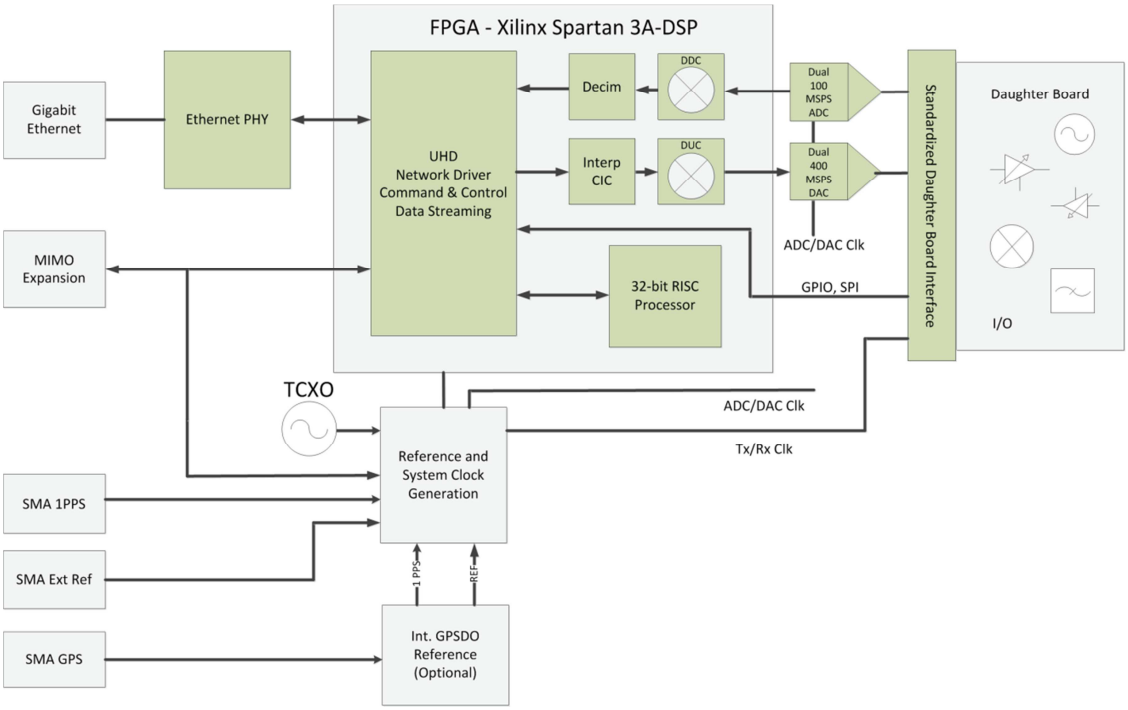


**Figure 3: Block diagram of USRP N210 provided by Ettus research**

## *2.1 As receiver*

The analog RF signal from antenna is converted to digital IF signal with 14 bit ADC of sampling rate 100 MSPS. Digital down convertor (DDC), implemented on FPGA, down converts the signal from IF to complex baseband, including the low pass filtering to remove the high frequency signal that is generated during down conversion.

After that, decimator reduces the data rate to make it compatible with LAN and computer (If the CPU is not fast enough, then data can be overwritten). The conversion from IF to complex baseband (quadrature modulation) is shown using an example (analog signal) below.

### 2.1.1 Quadrature demodulation

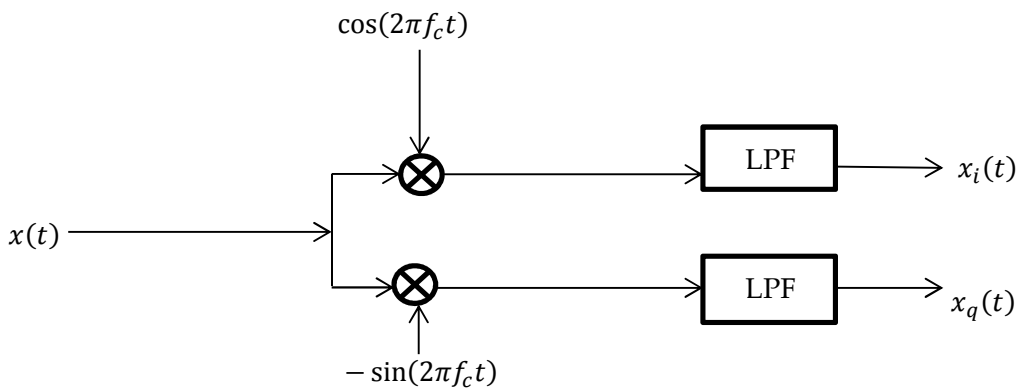


For a quick example, consider the original signal of the form below,

$$x(t) = 4cos(2\pi * 100t) + 5sin(2\pi * 110t) + cos(2\pi * 120t) + 7sin(2\pi * 130t) + cos(2\pi * 140t) + sin(2\pi * 150t) + cos(2\pi * 160t)$$

that has frequencies from 100 to 160 Hz with 10 Hz incremental. The bandwidth is from 100 to 160 Hz. To convert this signal to complex baseband signal, we need to multiply it with $e^{-i2\pi f_c t}$ (where$f_c$ = 130Hz) that will shift the spectrum around the center. Now, complex baseband signal is obtained by using low pass filter (since for example the frequency of $100 + f_c$ is also generated). The cosine component is in phase component and sine component is in quadrature phase. Therefore the in phase component is the low passed filtered $x(t) * \cos(2\pi f_c t)$. (Lathi 1998)

$$x_i(t) = 4cos\{2\pi * (100 - f_c)t\} + 5sin\{2\pi * (110 - f_c)t\} + cos\{2\pi * (120 - f_c)t\}$$
$$+ 7sin\{2\pi * (130 - f_c)t\} + cos\{2\pi * (140 - f_c)t\} + sin\{2\pi * (150 - f_c)t\}$$
$$+ cos\{2\pi * (160 - f_c)t\}$$

Similarly, low passed filtered $x(t) * \sin(2\pi f_c t)$ is quadrature phase component,

$$x_q(t) = 4sin\{2\pi * (100 - f_c)t\} - 5cos\{2\pi * (110 - f_c)t\} + sin\{2\pi * (120 - f_c)t\}$$
$$- 7cos\{2\pi * (130 - f_c)t\} + sin\{2\pi * (140 - f_c)t\} - cos\{2\pi * (150 - f_c)t\}$$
$$+ sin\{2\pi * (160 - f_c)t\}$$

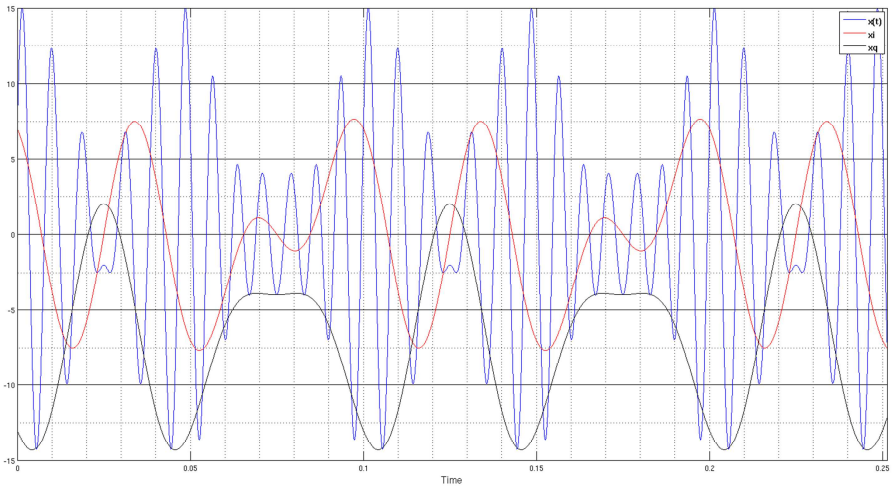


**Figure 4: Quadrature sampled signal; only requires half of Nyquist frequency to sample the signal**

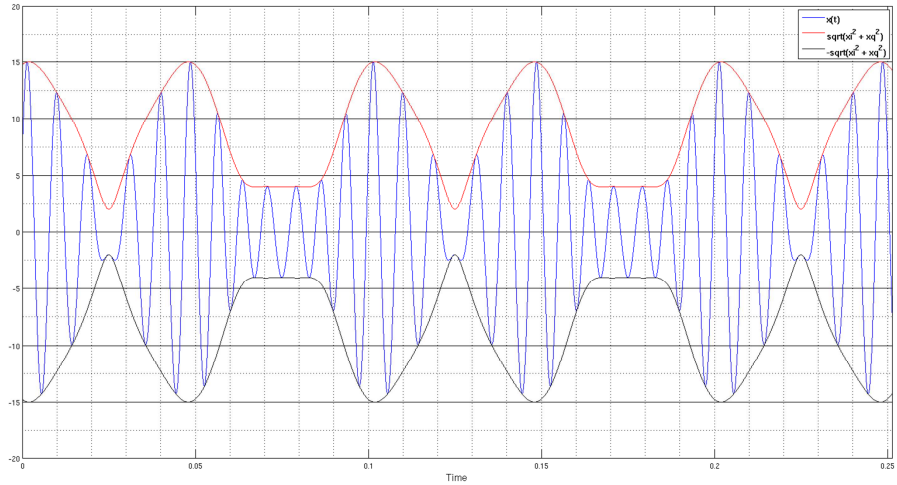


**Figure 5: Magnitude of $\sqrt{x_i^2 + x_q^2}$ is the envelope of the original signal $x(t)$, just like in amplitude modulation where $x(t)$ is carrier signal**

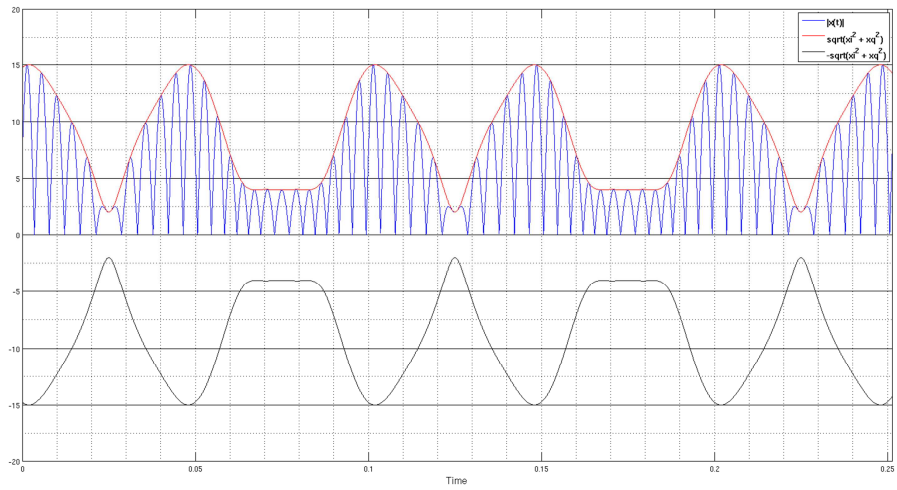


**Figure 6: Again magnitude of $\sqrt{x_i^2 + x_q^2}$ as the envelope of the absolute value of signal $x(t)$**

## *2.2 As transmitter*

Transmitter chain is exact opposite of the receiver. The complex baseband digital signal is required to be converted to IF signal. Interpolator increases the number of samples to increase the sampling rate for Nyquist criteria. Digital up convertor shifts the frequency spectrum to IF. 16 bit Digital Analog Convertor with 400 MSPS converts the signal to required RF analog signal. Now, for the analog signal the complex baseband to IF signal conversion is shown below as the reconstruction of the previous baseband signal. (The digital signal requires interpolator)

### 2.2.1 Quadrature modulation

To construct the original signal from $i$ and $q$, multiply the complex signal with $e^{i2\pi f_c t}$ to shift the spectrum to the center frequency of the original band limited signal and take the real part of the signal.

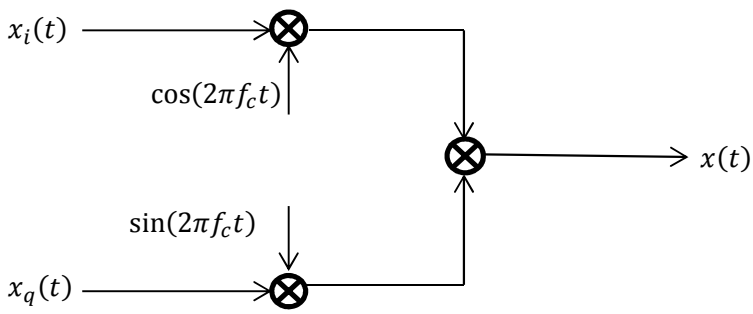


Now,

$x_{iq} = x_i + ix_q$

$x(t) = Re(x_{iq} e^{i2\pi f_c t})$

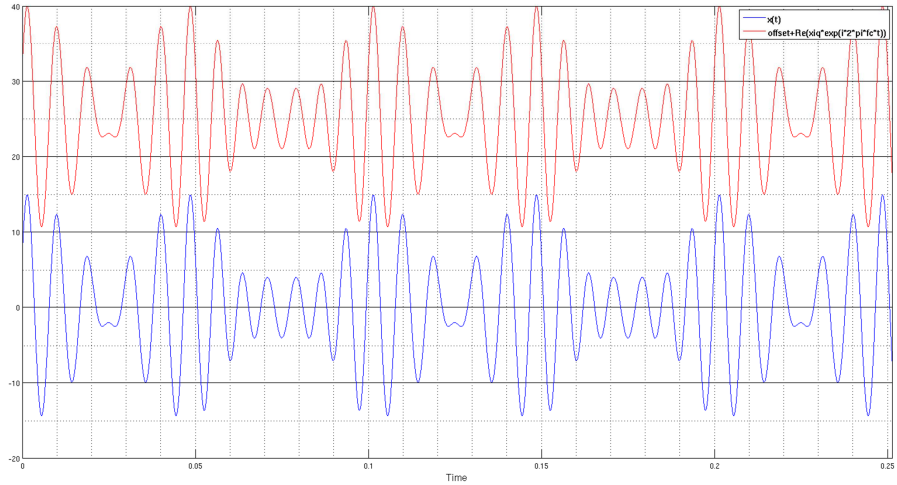


**Figure 7: Reconstruction of the original signal, here an offset is added to distinguish two plots which are exactly same**

## *2.3 GPS integration*

The two ways to incorporate GPS clock and timing to USRP N210 are either by using internal or external GPS disciplined oscillator. The output of external GPS receiver, 1 PPS and 10MHz reference clock, can be connected to the respective front panel SMA connectors of USRP. However, USRP requires NMEA (National Marine Electronics Association) reference frames to decode absolute GPS timing. If only the clock accuracy is required, RS232 serial connection (NMEA) is optional. An example of RMC NMEA frame from Figure 9 is following,

$GPRMC,201505.00,A,3558.2461,N,7905.6592,W,0.0,0.0,080711,,*14

Where 201505.00 is UTC time (20:15:05.00), A indicates that data is valid (otherwise V), 3558.2461N is latitude and 7905.6592W is longitude. Then 0.0 is the speed over ground and 080711 is the date.

Therefore, internal GPSDO provided by Ettus Research which has RS232 serial output was used in the project. The block diagram is as follows. (Serial output of many external GPS receivers is just UTC time instead of NMEA frame e.g. Truetime's XL-AK).

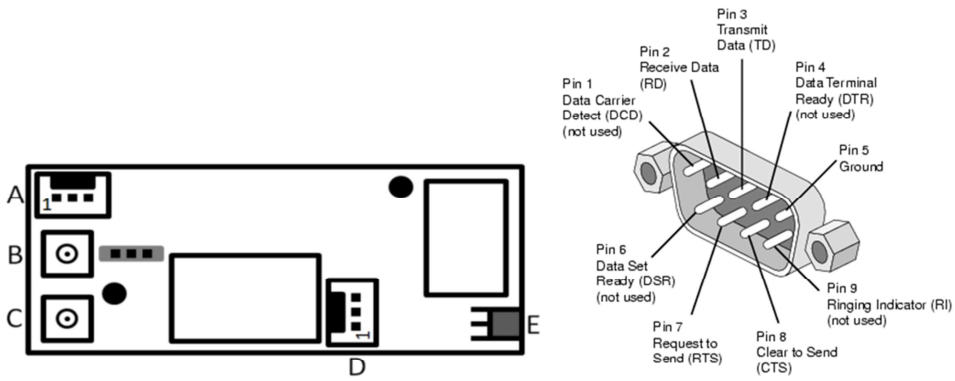


**Figure 8: On the left, block diagram of internal GPSDO provided by Ettus research, where (A) RS232 (B) 1 PPS (C) 10MHz reference clock (D) Power (E) GPS antenna. On the right, RS232 DB9 pin out (adapted from wiki.robotz.com)**

There are multiple ways to check whether GPS is locked or not. One of them is to use serial communication to verify the NMEA frames and that can be done as follows. Connect the RS232 output of the internal GPSDO to RS232 DB9 serial port of the computer (Refer to the pin configuration of RS232 DB9 and GPSDO's pin configuration). Serial port to USB connector can be used in the absence of RS232 DB9 port on computers (Usually laptops). Use HyperTerminal to receive the NMEA frames transmitted by

GPSDO. Serial communication parameters of internal GPSDO are as follows: 115.2K baud rate, 8 data bits, no parity and 1 stop bit.

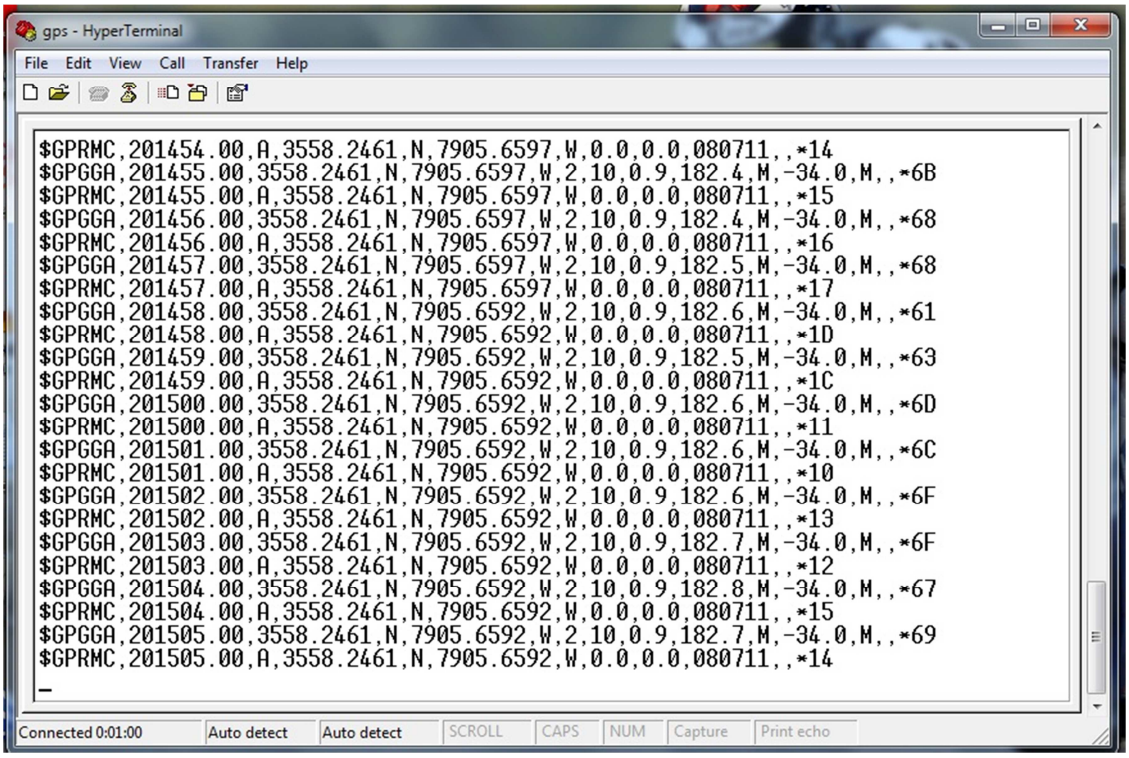


**Figure 9: Using HyperTerminal to receive the NMEA frames transmitted by internal GPSDO**

# 3. Setup

For reception of EM radiation produced by lightning, a Discone omnidirectional antenna, receiving range of 70 MHz to 3 GHz, was utilized. For GPS signal reception, active GPS antenna by symmetricom was used. The daughterboard TVRX2 (50-860MHz, receiver only) was used most of the time. Data from SBX (400-4400MHz, transceiver) was omitted due to various issues such as internal noise and *i-q* imbalance (even after calibration utility). To program the USRP N210 for streaming the data with absolute timings or synchronizing two USRP, C++ programs from UHD's application programming interface (API) were made. The UHD documentation can be found in the following link.

http://files.ettus.com/uhd_docs/doxygen/html/index.html

In UHD, the absolute time is displayed as UNIX time (seconds since January 1st, 1970). Previously, querying the motherboard sensor via UHD API for absolute time displayed GPS time (seconds since January 6th, 1980). The difference between GPS time and UTC time is the 16 leap seconds. To keep the atomic clocks synchronized to slight slowing of earth's rotation, the International Earth Rotation and Reference Systems Service (IERS) adds leap seconds (one leap second added at June 30th, 2012) to UTC time.

Recorded complex samples *I* and *Q* are 32 bit float. Therefore, one sample means 32 bit *I* and 32 bit *Q*. The absolute time of the first sample is known so the absolute time

of the any sample can be known immediately according to the sample rate. From total number of bytes in recorded file, the total time of streaming is known.

In two radio configuration, MIMO cable was utilized previously. USRP N210 (as master) and USRP 2 (as slave) were connected via MIMO cable in dual Ethernet mode. USRP 2 didn't support internal GPSDO so the GPS clock and timing were communicated over MIMO cable. Later, two USRP N210 with independent GPSDO were utilized. For both the configurations, same Discone antenna was used. To split the output from the same antenna, 3dB power divider (5MHz to 2GHz), which is basically Wilkinson power divider with broadband frequency response, was used. Measurements with same frequency, same bandwidth and at same location were taken to see the saturation range, internal noise and absolute timings of two USRP. The USRP N210 input impedance is 50 Ω and so no reflection waves (voltage and current) were found inside the transmission lines connecting the systems with the antenna. USRP has programmable gain amplifier so different gain settings can be set using UHD API.

One problem worth writing occurred with SBX daughterboard. The problem would explain spectrum of complex signal. Now from Euler formula,

$e^{i\theta} = cos\theta + isin\theta$, so $cos\theta = \frac{e^{i\theta}+e^{-i\theta}}{2}$ and $sin\theta = \frac{e^{i\theta}-e^{-i\theta}}{2i}$

For in phase component in Quadrature sampling, the signal is multiplied with $cos\omega_c t$ which has even spectrum (from Euler's formula, positive and negative frequencies are of same magnitude), while for quadrature phase component, the signal

is multiplied with $sin\omega_c t$ which has odd frequency spectrum (from Euler's formula, positive and negative frequencies are of opposite magnitude). Therefore when $cos\omega_c t$ is added with $(isin\omega_c t)$, the original frequency is obtained. However, if the in phase or quadrature phase component is missing or malfunctioning, the final spectrum would be even or odd function of the original spectrum respectively. In the SBX daughterboard, the quadrature phase signal was missing, therefore the mirror image of the frequency was seen in the spectrum.

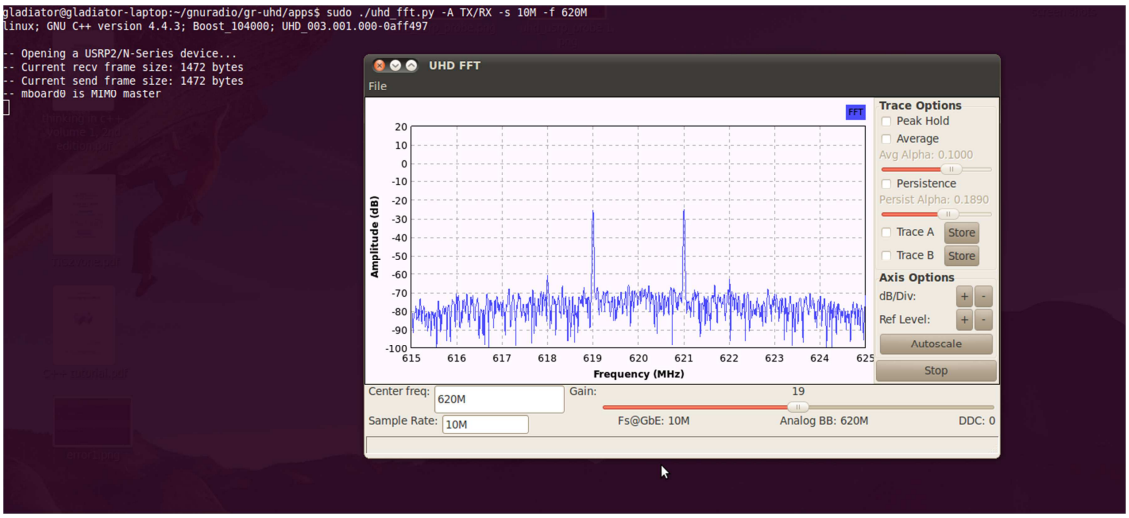


**Figure 10: Signal transmitted at 621MHz but the spectrum shows reception at 619MHz as well; spectrum is complex baseband but original frequencies are displayed for convenience**

# 4. Measurements with 0 dB gain

Measurements were taken at Duke Forest with single USRP N210 (UHD) and TVRX2 daughterboard (50-860 MHz) at VHF (67-75 MHz) and UHF (695-715 MHz) with 0dB gain. TVRX2 supports 10MHz bandwidth; however, the computer receiving the data through LAN couldn't process the incoming data-rate more than 2 MSPS (data overrun otherwise). Therefore, recordings were done with 2MHz bandwidth and continuous streaming time of 2-3 minutes was given to each frequency band (e.g. 67-69 MHz, 69-71 MHz). National Lightning Detection Network (NLDN) provided the location (latitude and longitude), time (UTC with 0.1 millisecond accuracy), peak current and type of lightning flashes occurred. Following is the lightning distribution plot from NLDN data compared with our VHF data to evaluate our system. With 0dB gain, many processes in a lightning flash were diminished inside noise so higher gain measurements were essential.

Location: Duke Forest lab, 35.9708N -79.0943E

## *4.1 VHF (67-75 MHz)*

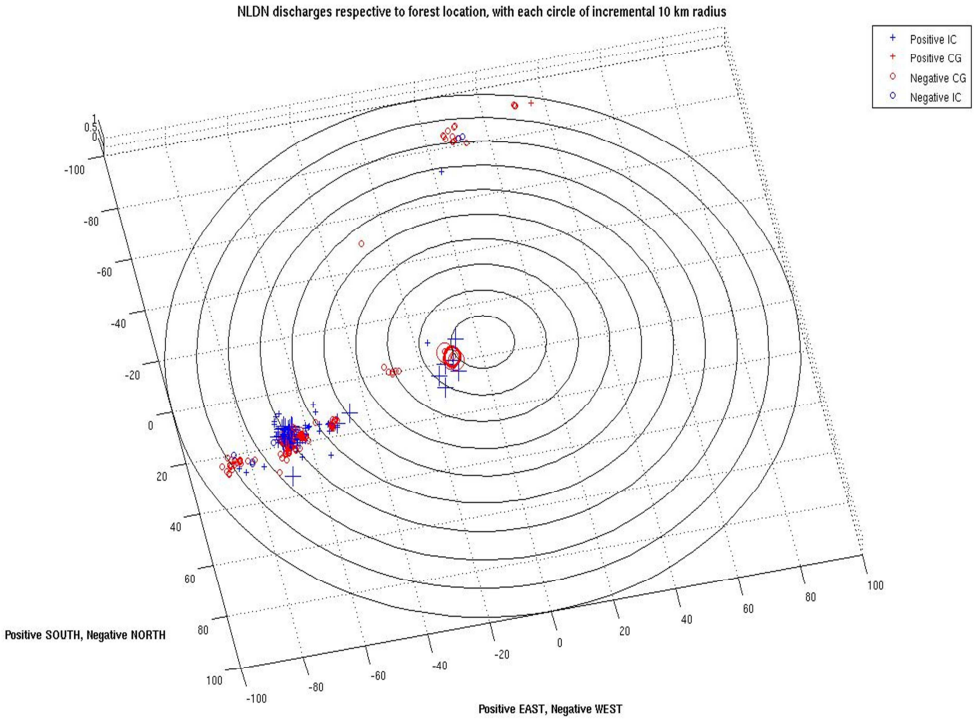


**Figure 11: Larger marker sizes indicate that the corresponding NLDN lightning flashes are detected in our system (VHF) and vice versa; in the plot, grid lines don't represent constant latitude, longitude circles, instead these circles have same trajectories as in astronomy charts**

As can be seen from the plot, cloud to ground discharges were only detected inside 20 km. Moreover, the peak of the return stroke was not detected at VHF with 0 dB gain. The highest magnitude processes at VHF didn't correspond to a return stroke. Following are the VHF-LF plots from cloud to ground discharge.

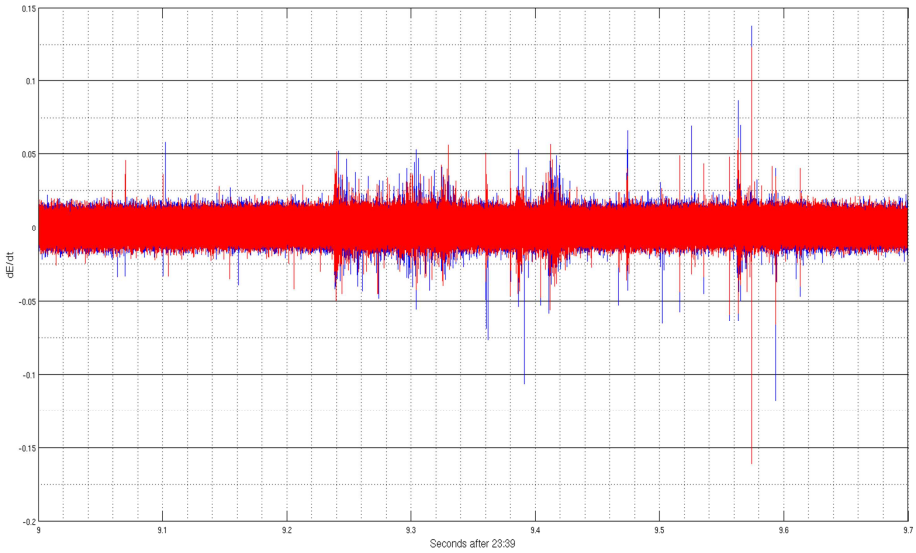


**Figure 12: recorded at 73-75 MHZ with 0dB gain (|noise level|< 0.02), NLDN info: event time (first return stroke) 23:39:9.359 (UTC), CG at 12.7175 km with -20kA peak current**

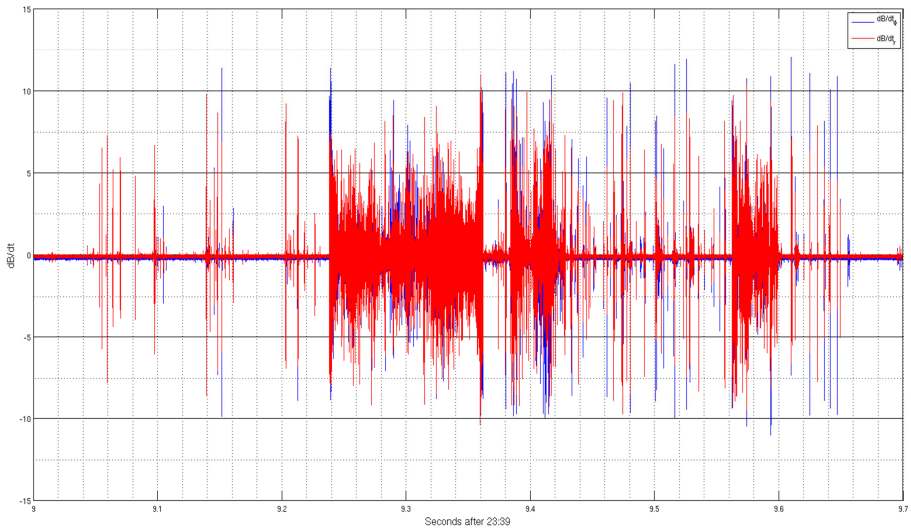


**Figure 13: Corresponding LF plot**

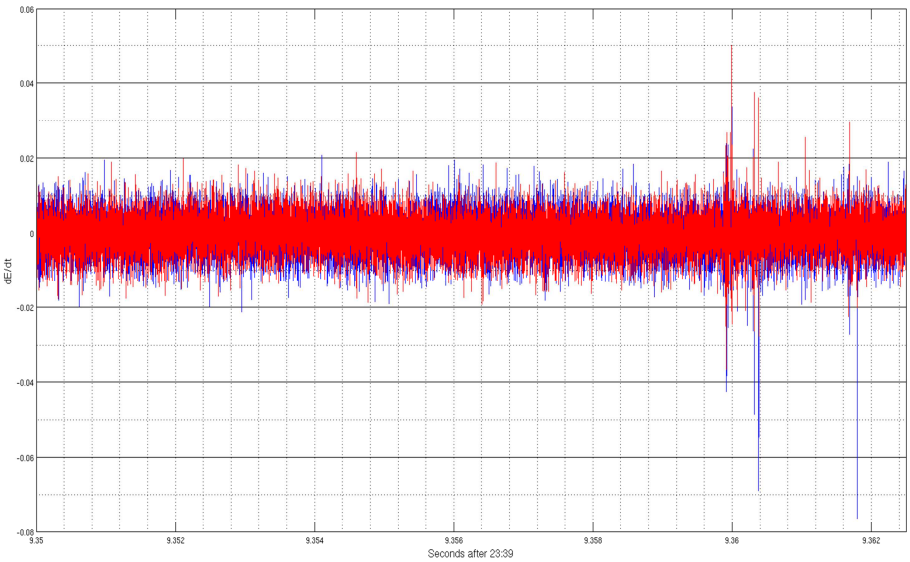


**Figure 14: First return stroke, not producing highest $\frac{\partial E}{\partial t}$ during flash; next pulses may correspond to fine structure (Davis 1999)**

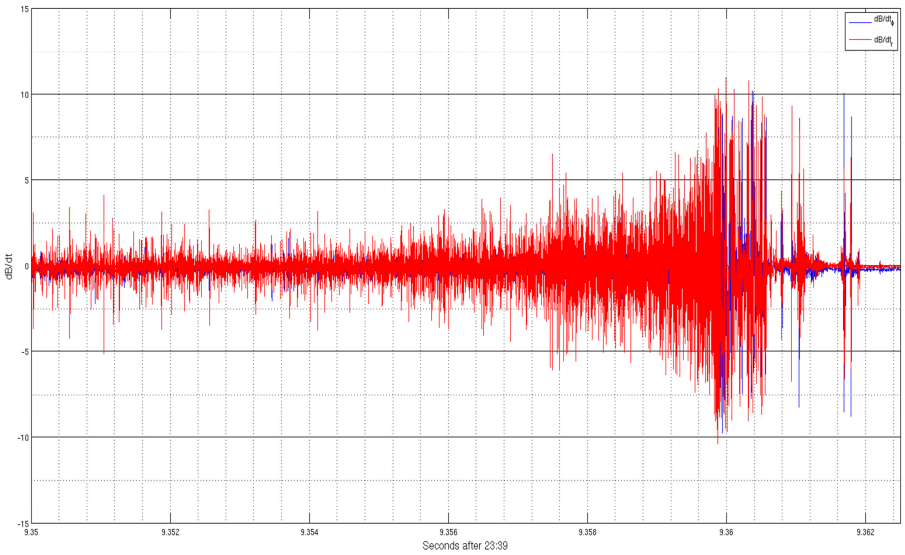


**Figure 15: First return stroke at LF**

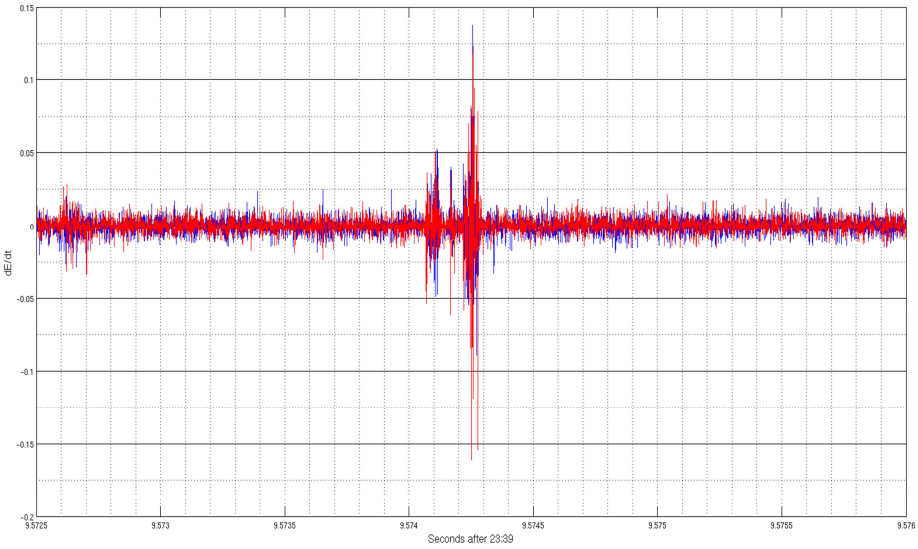


**Figure 16: Highest $\frac{\partial E}{\partial t}$ during entire flash**

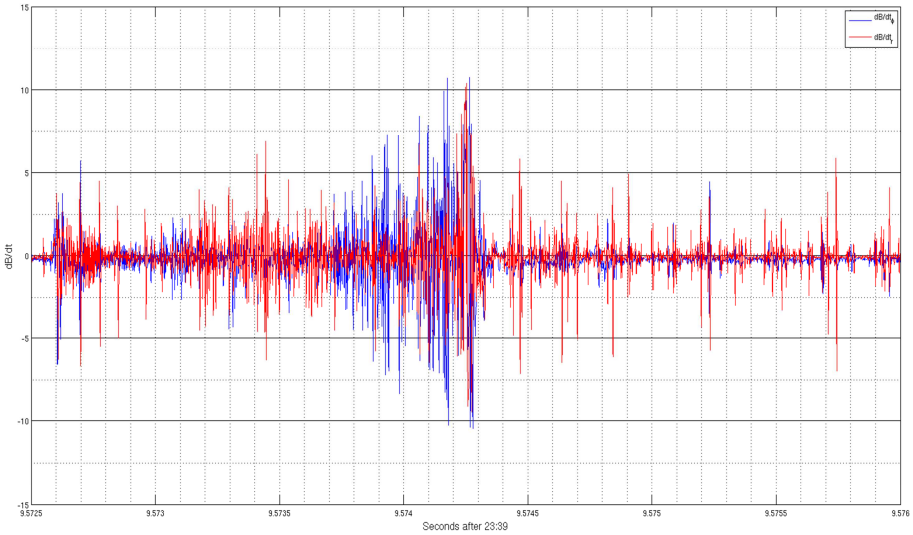


**Figure 17: Corresponding LF plot; this process cannot be a subsequent return stroke due to the continued small pulses extending beyond the time window of the plot**

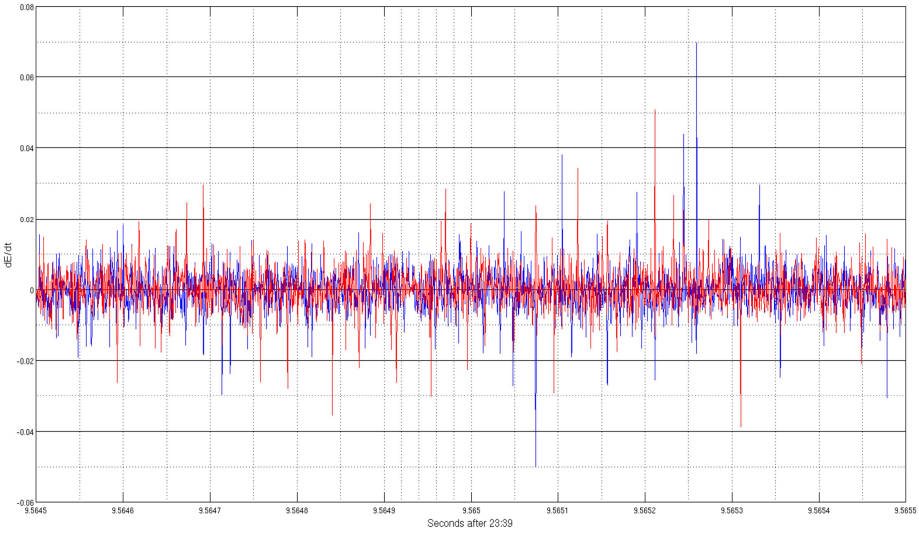


**Figure 18: Probably the regular pulse bursts occurring before the highest $\frac{\partial E}{\partial t}$ event**

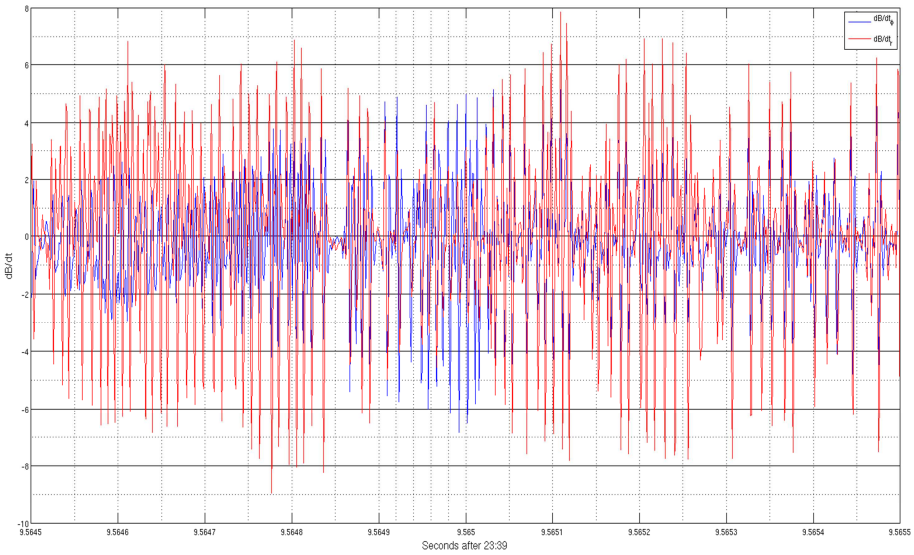


**Figure 19: Corresponding LF plot**

For cloud discharges at close range (inside 30 km), some of the K processes with lower magnitude at LF were not detected at VHF. However, K processes, may be superimposed on J processes of higher magnitude at LF, were clearly visible at VHF. Magnitude comparison of VHF ($\sqrt{\boldsymbol{i}^2 + \boldsymbol{q}^2}$) and LF ($\sqrt{\frac{\partial \boldsymbol{B}}{\partial \boldsymbol{t}_{\boldsymbol{r}}}^{2} + \frac{\partial \boldsymbol{B}}{\partial \boldsymbol{t}_{\emptyset}}^{2}}$) isn't presented, since LF signal was saturated due to close lightning, while only few pulses were close to saturation for VHF. The detailed description of IC is presented in last section.

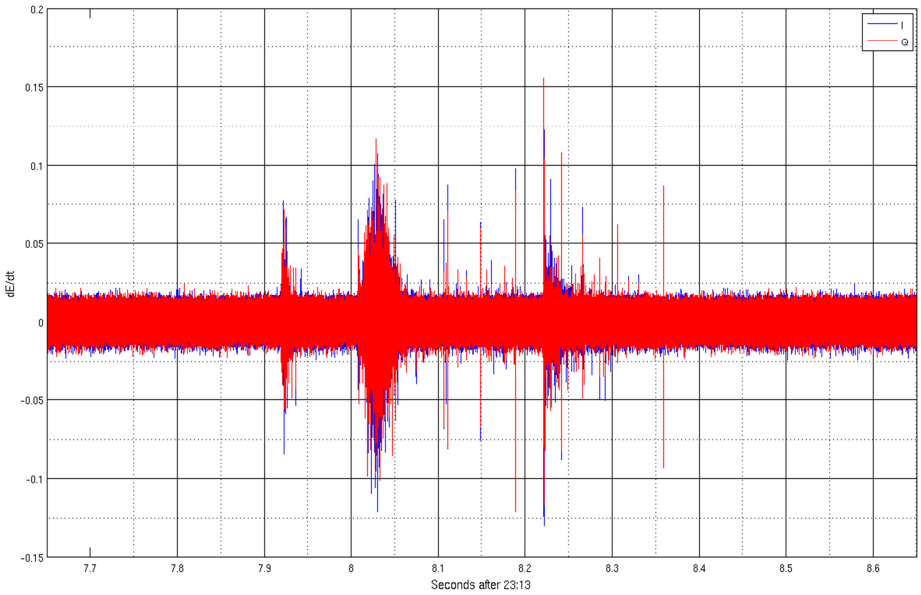


**Figure 20: Recorded at 67-69 MHz (|noise level| < 0.02). NLDN info: event time 23:13:8.221 (UTC), IC at 8.5838 km with 12kA peak current**

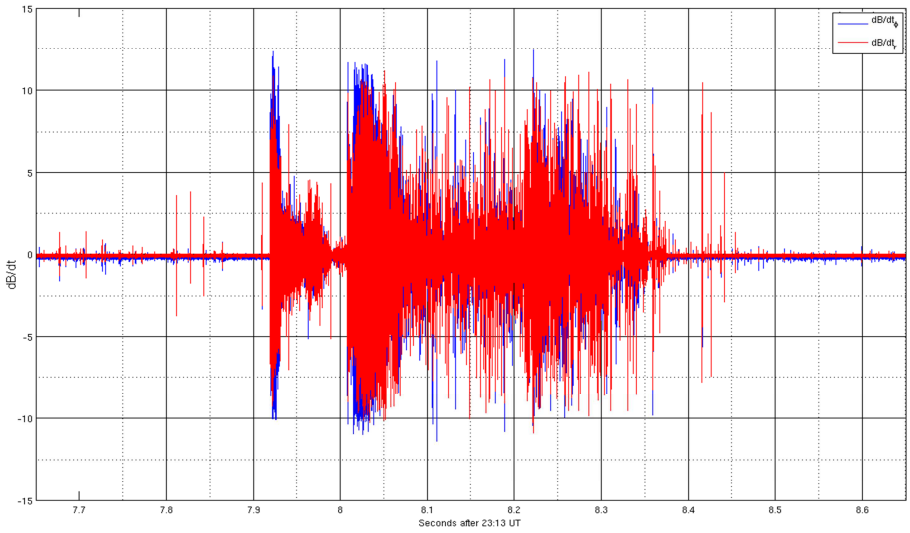


**Figure 21: corresponding LF plot, no other close lightning flash in the plotted time window**

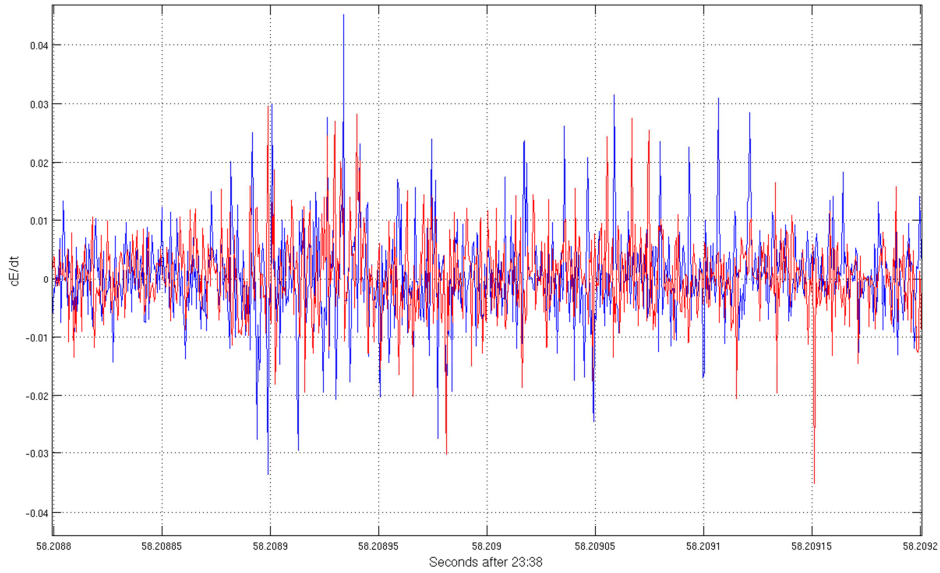


**Figure 22: K processes with higher magnitude at LF were detected at VHF. This plot shows (recorded at 73-75 MHz) IC at 14.3904 km with 9kA peak current, occurring at 23:38:57.988**

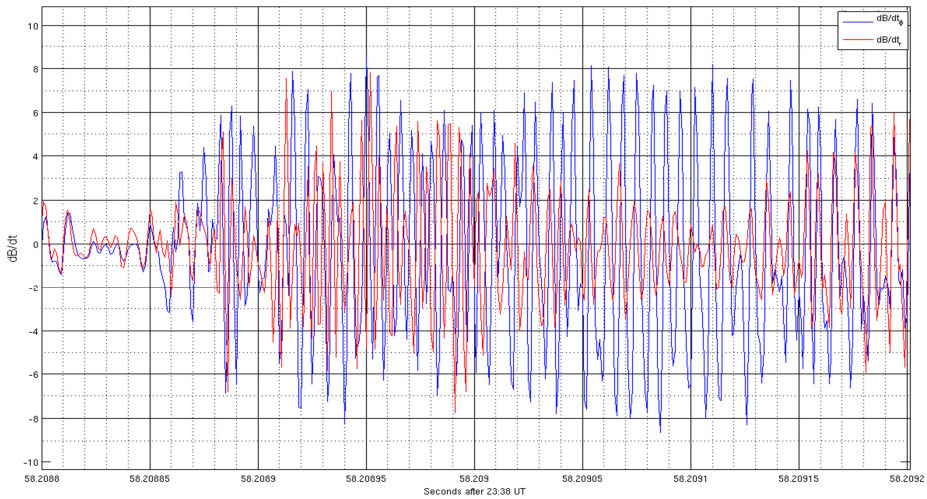


**Figure 23: Probably the K process superimposed on slower (electric field change) J process producing higher magnitude**

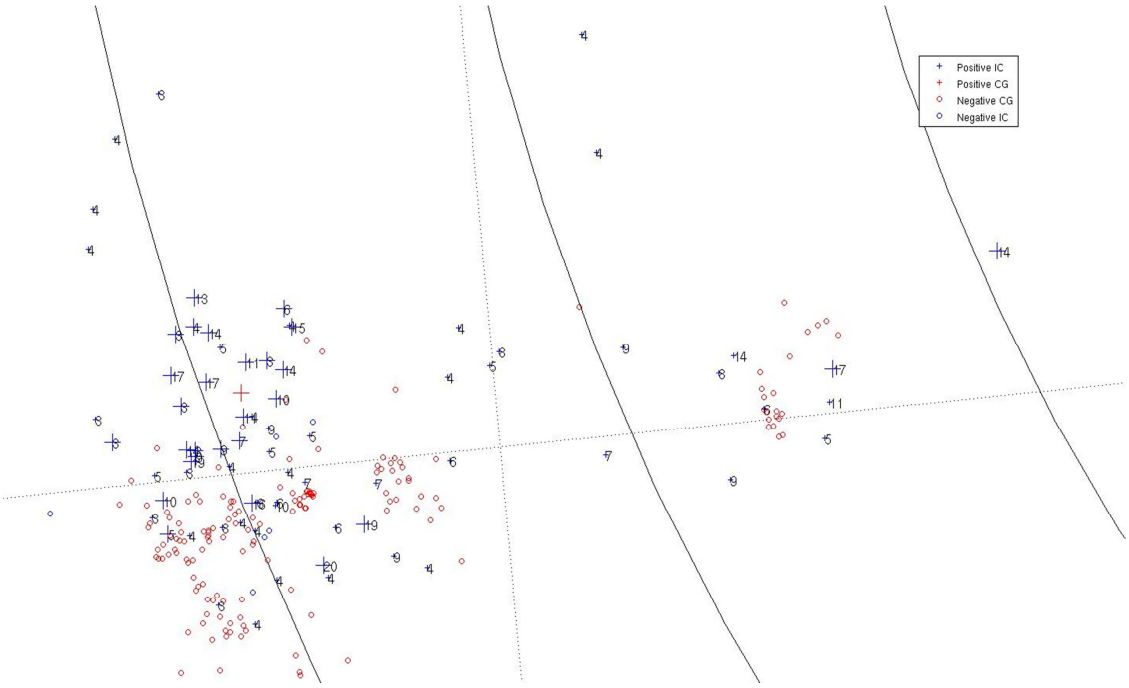


**Figure 24: Closer look at the plot in Figure 11; left most part of circle is at 70 km away from lab in Duke forest, similarly consequent circles to right are 60 and 50 km away respectively. The numbers associated with positive IC are peak currents provided by NLDN**

Some of the cloud discharges at 70 km with smaller currents were detected at VHF, while some at 50 km with higher currents were not detected (Figure 24). Initial guess was to check the height of the origin of flash. However, by checking the waveforms of all detected and undetected flashes, it turned out that all the detected flashes were narrow bipolar events (Le Vine 1980) producing strong HF-VHF radiation. These pulses had time duration of 10-15μs at VHF and ranged from 20 to 100μs for LF. While the cloud discharges, undetected in VHF systems, were typical IC with active and final stage. Typical IC detection range should be somewhere in between 20 to 50km. The storm didn't produced lightning at intermediate range (Figure 11) and the one IC that occurred

at around 48km was a narrow bipolar event. None of the ionospheric reflections were detected at VHF-UHF. However, these reflections were present at LF.

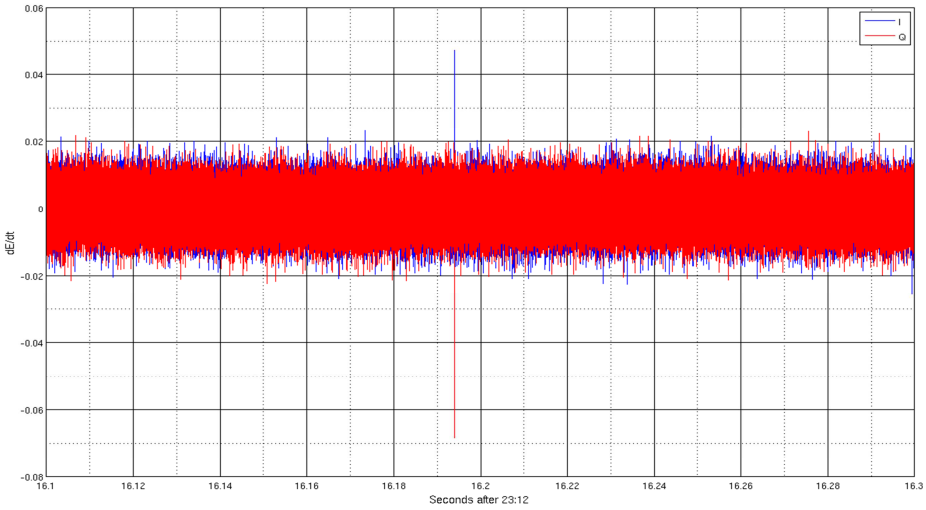


**Figure 25: Recorded at 67-69 MHz; IC occurring at 23:12:16.193 (UTC) with 9kA current at 70.01 km**

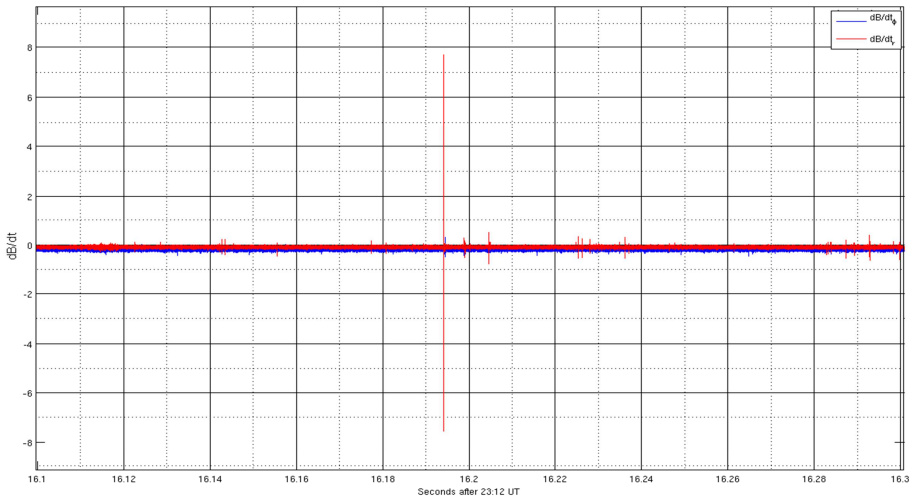


**Figure 26: Corresponding LF plot; no other flash in the plotted time window**

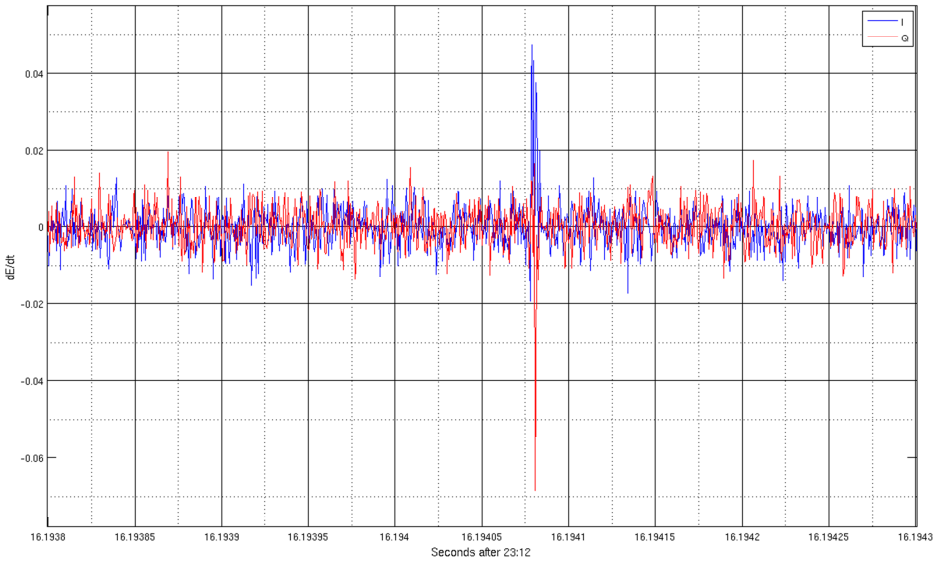


**Figure 27: Zoomed in VHF plot, pulse duration is ~10 µs consistent with (Le Vine 1980)**

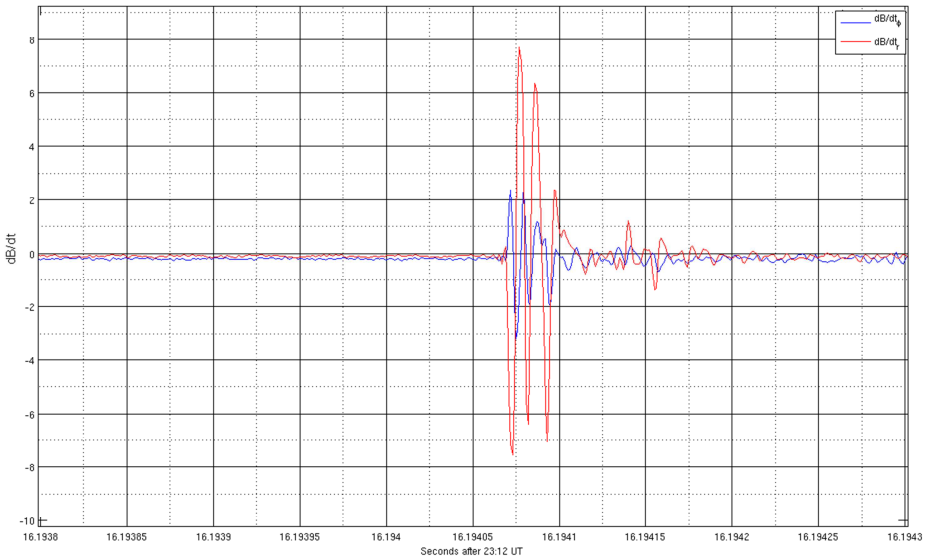


**Figure 28: Corresponding LF plot with pulse duration of ~60µs**

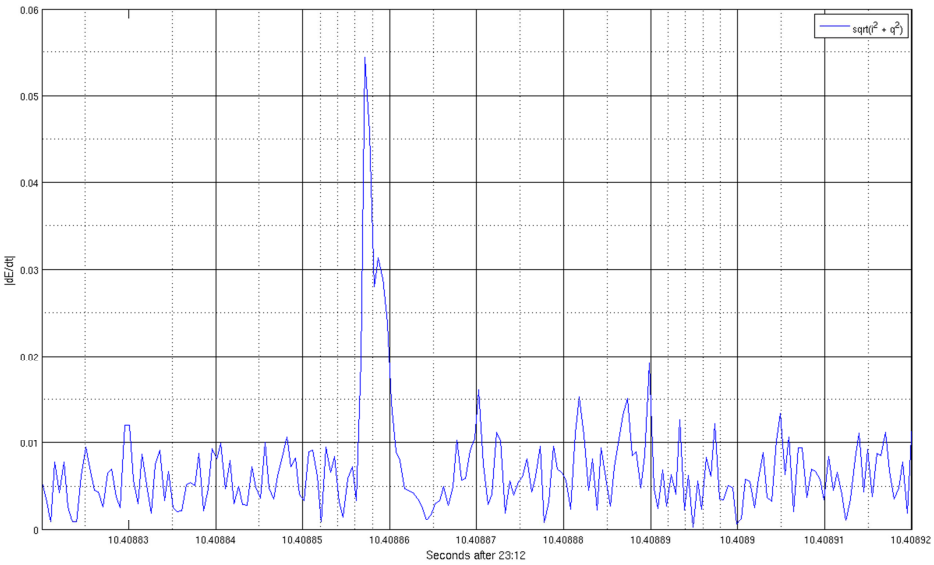


**Figure 29: Narrow bipolar event (at 70.64 km with 3kA peak current). Here absolute value of RF signal follows the envelope $\sqrt{\mathbf{i^2 + q^2}}$**

Now the following plots show LF waveforms of undetected IC.

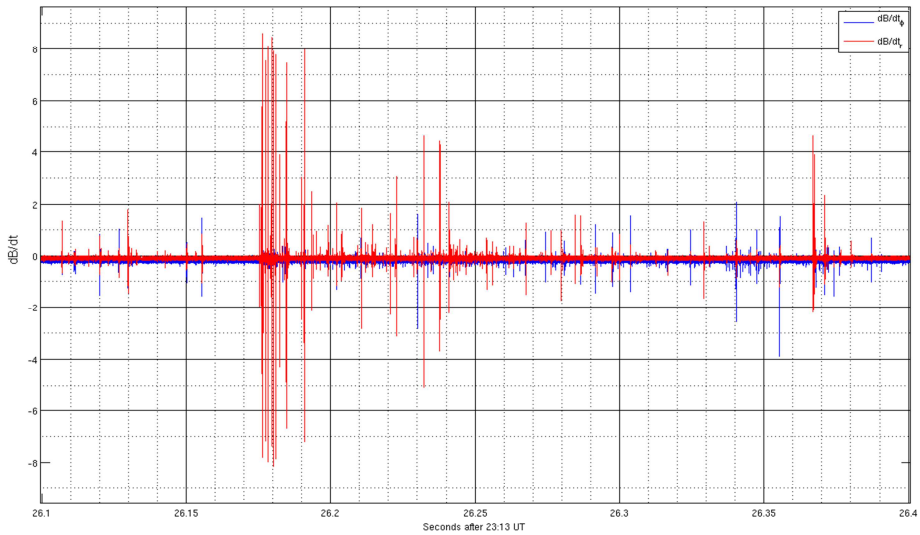


**Figure 30: Typical IC (with Active and final stage) at distance 55.49 km which wasn't detected at VHF, strongly suggesting the detected IC as narrow bipolar events**

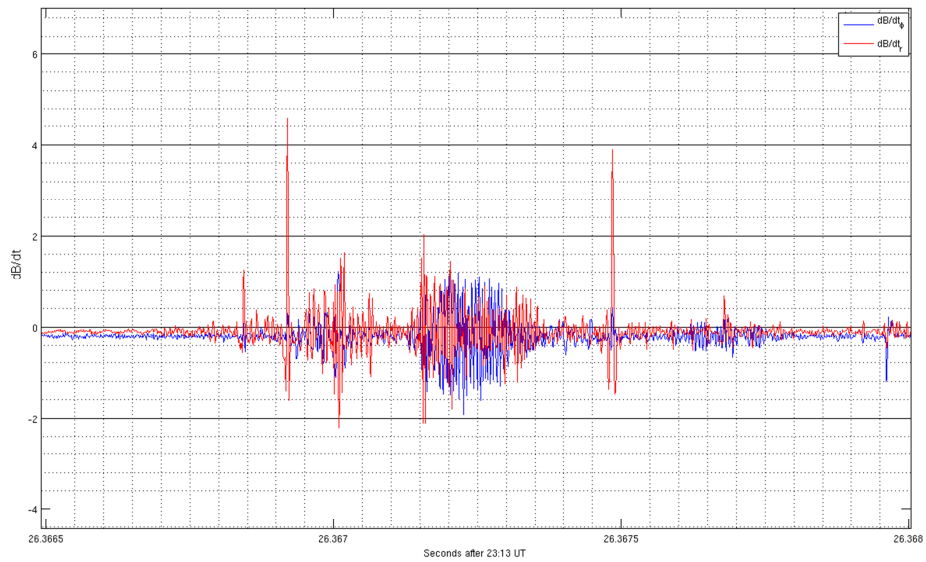


**Figure 31: Probably K process occurring at final stage of the IC in Figure 30**

Now, following are the plots for magnitude distance relationship in IC and CG.

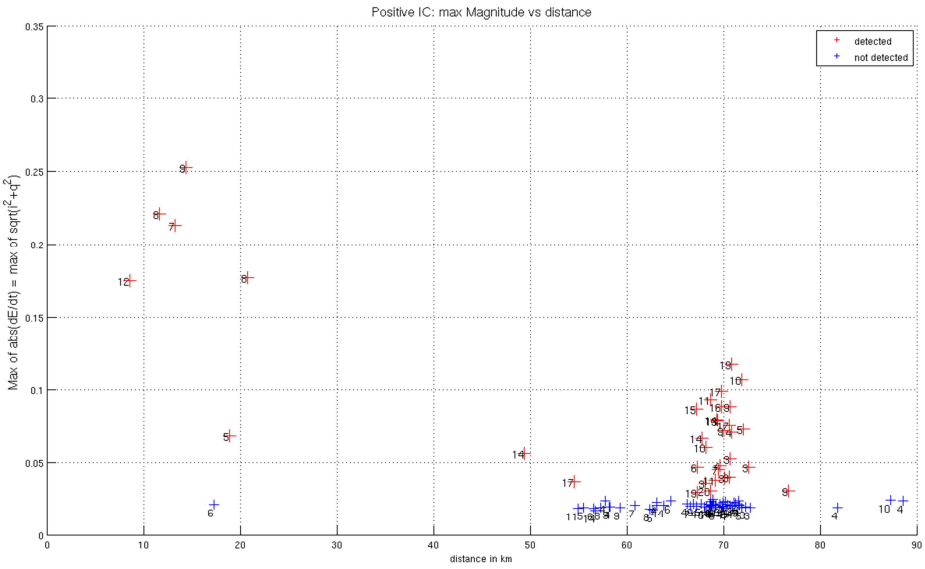


**Figure 32: Maximum of $|\frac{\partial E}{\partial t}|$ for positive IC in time duration = min $\{1\text{sec}, \frac{d_{i-1}}{d_i + d_{i-1}} t_1 + \frac{d_{i+1}}{d_i + d_{i+1}} t_2\}$ where $t_1$ and $t_2$ is time (seconds) between two NLDN events, while $d_i$ is the distance of $i^{th}$ event from Duke Forest**

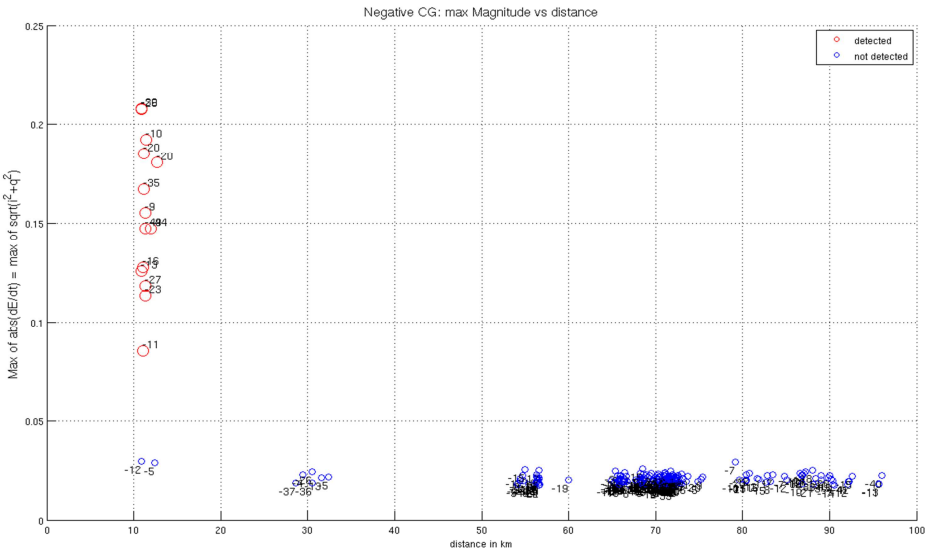


**Figure 33: Similarly for negative CG**

## *4.2 UHF (695-715 MHz)*

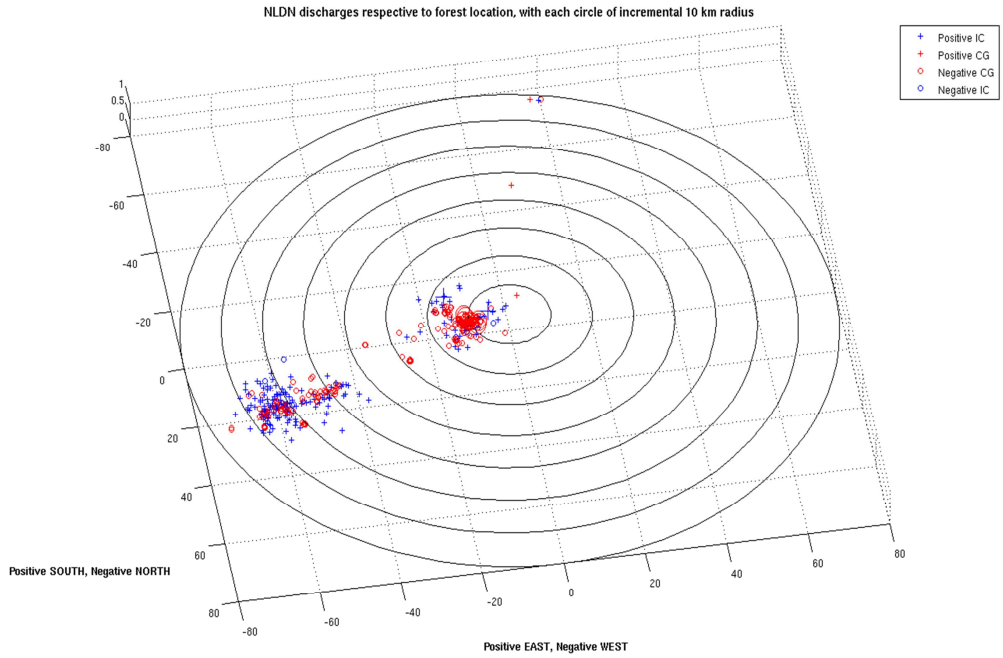


**Figure 34: Larger marker sizes indicate that the corresponding NLDN lightning flashes were detected in UHF system and vice versa; in the plot, grid lines don't represent constant latitude, longitude circles, instead these circles have same trajectories as in astronomy charts**

Only two IC were detected and one of them occurred during LF dead time window. From analysis of the waveforms, the other IC was a narrow bipolar pulse. In all detected cloud to ground discharges, the return strokes didn't produce any UHF pulses at all for 0 dB gain. Follow the plots below for UHF pulses.

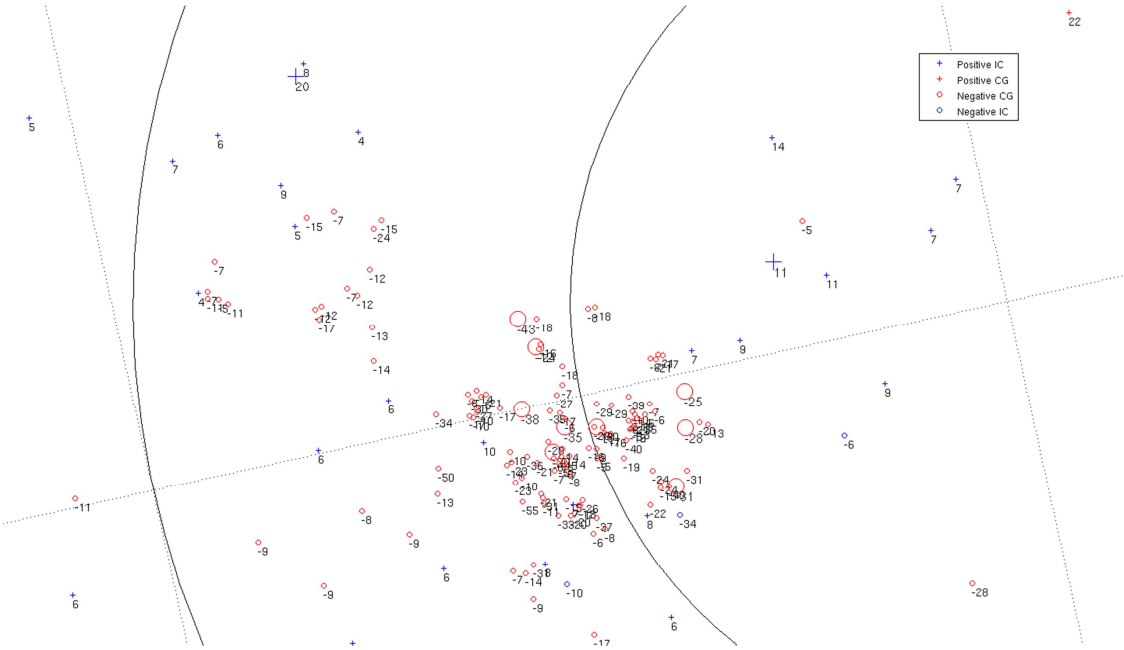


**Figure 35: Closer look at the plot in Figure 34; left most part of circle is at 20 km away from lab in Duke Forest, similarly next circle at right is 10 km away. The numbers associated with positive IC are peak currents provided by NLDN.**

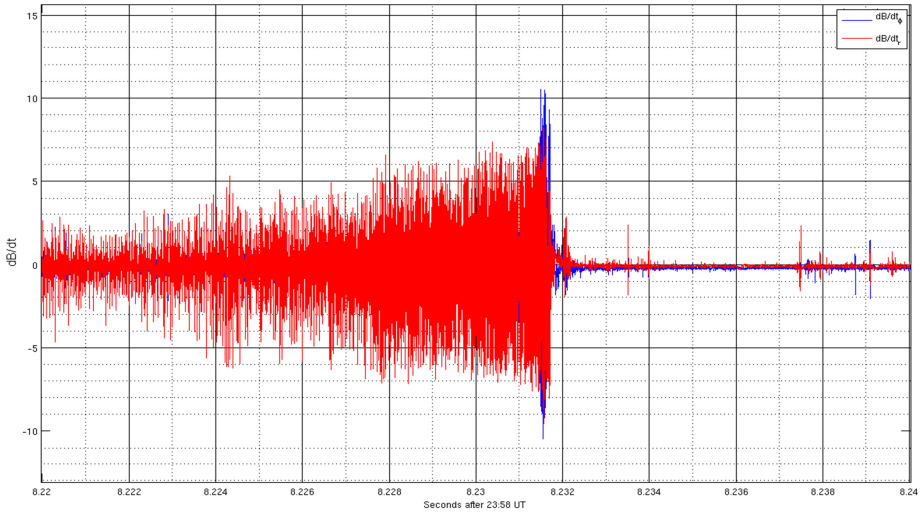


**Figure 36: Return stroke, undetected at UHF with 0 dB gain and 2 MHz bandwidth (-29 kA peak current and 9.3675km distance for the plotted CG)**

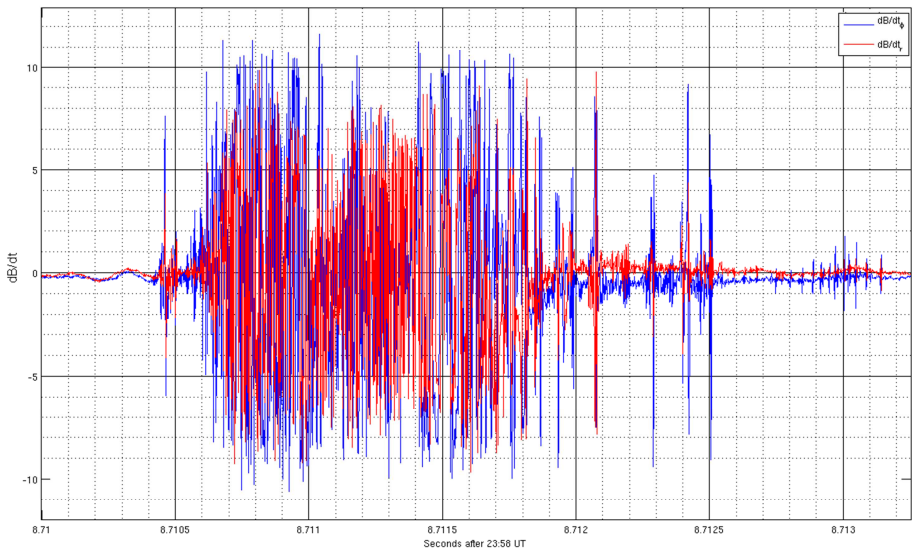


**Figure 37: Similar CG processes in NLDN time window which were undetected at UHF (-29 kA peak current and 9.68 km distance for the plotted CG)**

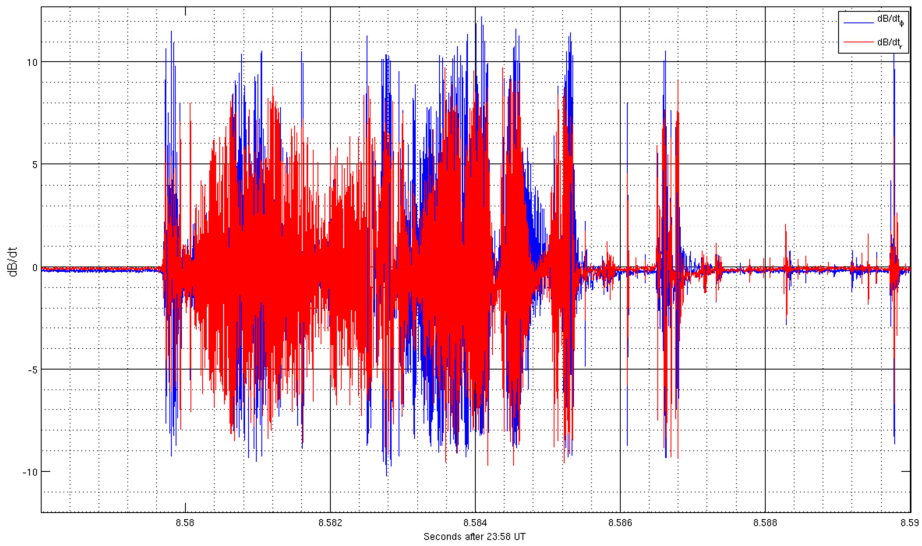


**Figure 38: CG processes inside NLDN time window, detected at UHF. The time duration of such processes were ranging from around 0.003 to 0.06 seconds (-13 kA peak current and 9.83 km distance for the plotted CG)**

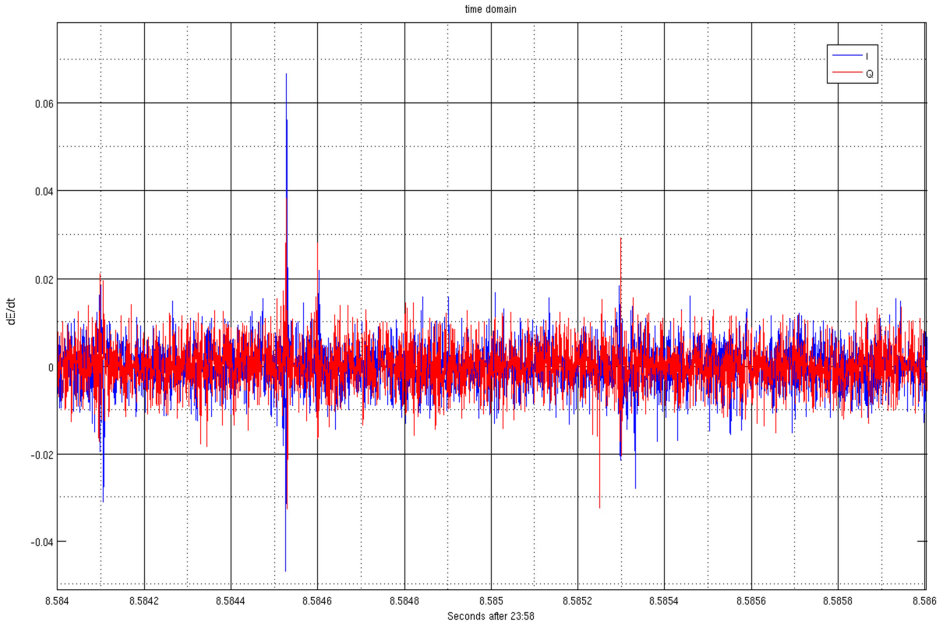


**Figure 39: UHF (713-715 MHz) activity of the CG**

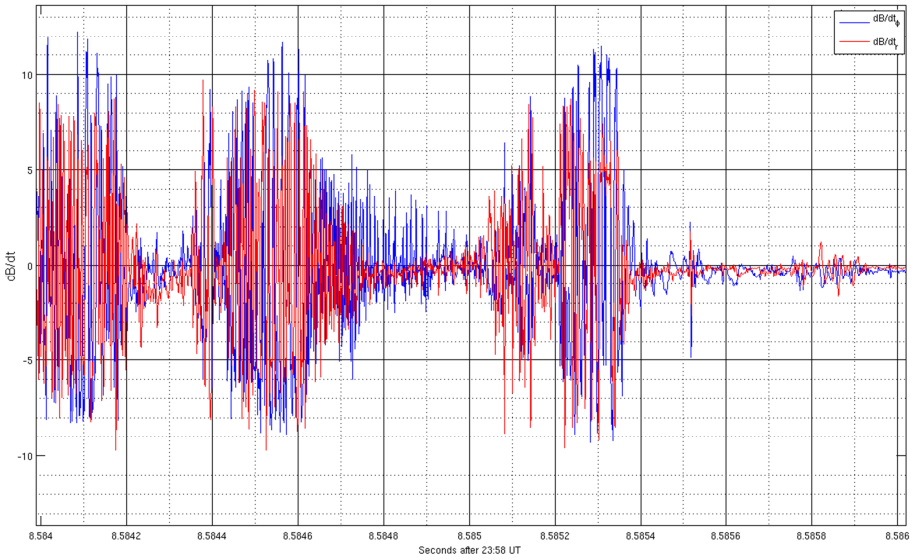


**Figure 40: Corresponding LF plot**

# 5. Measurements at higher gain

Simultaneous VHF-UHF measurements were taken using MIMO cable in dual Ethernet mode. Therefore, two computers were connected to two USRP (sharing clock and timing via MIMO cable) via separate LAN cables. The USRP2 doesn't support internal GSODO and external GPS receivers only provide the 1PPS and 10MHz signal, no serial output (NMEA frames). Therefore, to incorporate GPS timing as well as clock, MIMO cable was utilized. Unfortunately, MIMO sync to slave turned out to be inaccurate via comparing the lightning signal at VHF with LF and NLDN. All the VHF (TVRX2 with USRP2) recordings were delayed in time (~0.02047 sec) and the time delay wasn't exactly constant over the same recording, questioning the clock and PPS sync as well. The daughterboard SBX, connected to USRP N210 for UHF measurements, was not reliable due to clock spurs occurring in recordings. Therefore, UHF data is not presented here.

About the storm at 17$^{th}$ November 2011, many of the cloud discharges were observed and received at VHF and LF. However, the NLDN omitted many of such flashes. Measurements were taken at two different gain settings. Following is at 8dB.

## *5.1 With 8 dB*

The positive IC occurring inside 20 km in the Figure 41 was detected (with few others as well) at VHF but due to impreciseness of MIMO clock and time synchronization, the comparison to NLDN is not plotted by larger marker size.

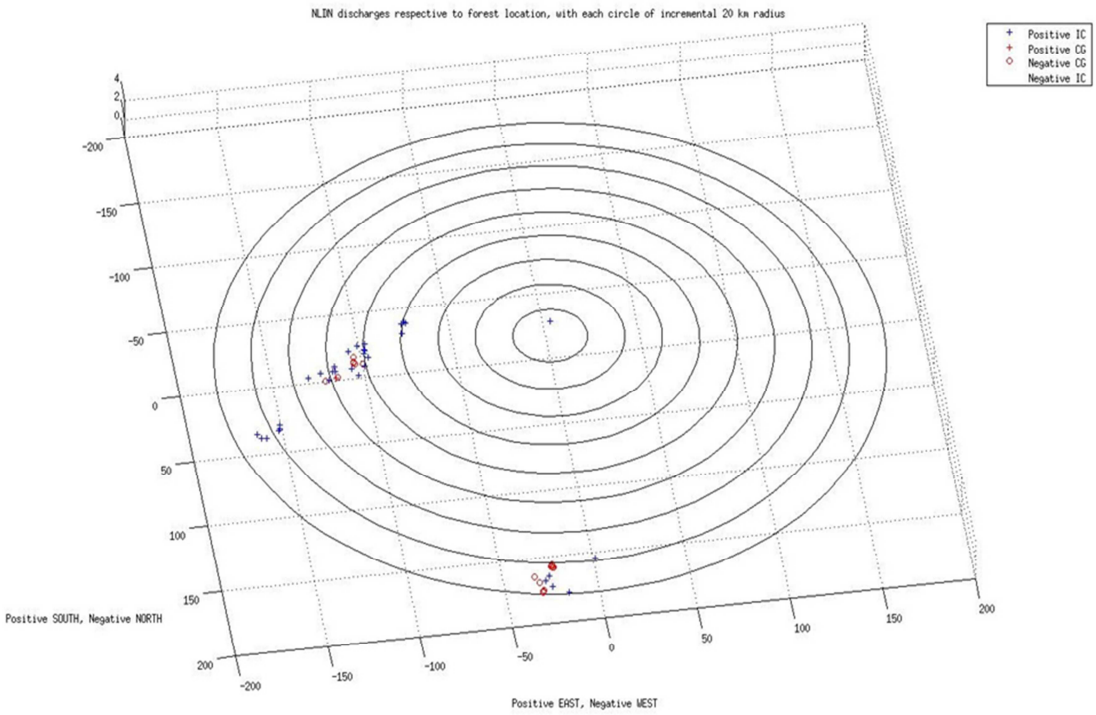


**Figure 41: Each circle with 20 km incremental radius. Events are not displayed that happened during the noisy recordings. No symbol for Negative IC (in legend) means none occurred during the measurements**

## *5.2 With 16 dB*

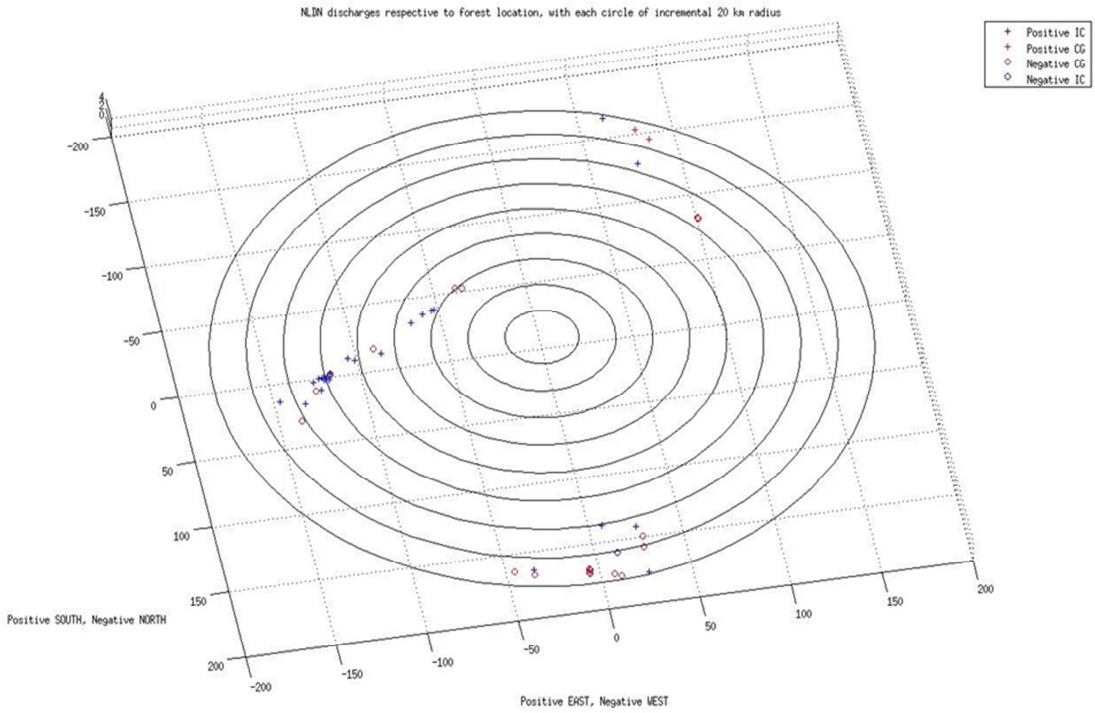


**Figure 42: Each circle with 20 km incremental radius; again due to impreciseness of MIMO sync, VHF data wasn't compared with NLDN. Events occurred during noisy recorded data were omitted.**

The plots for cloud discharges at VHF and LF were quite similar. However, the magnitude comparison at microseconds scale differed in many ways. Such behavior is documented in the last section.

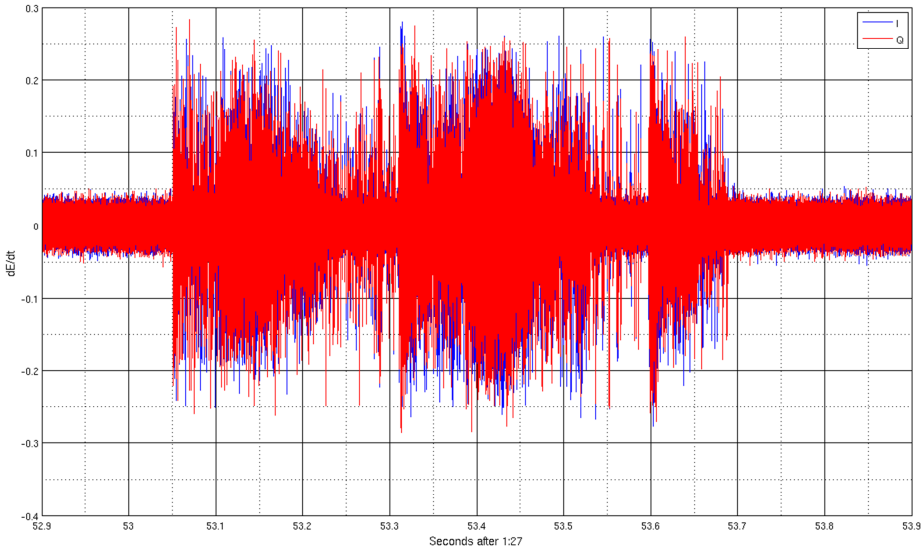


**Figure 43: Recorded at 71-73 MHZ with 16dB gain. Positive IC not reported by NLDN but should be at close distance (VHF saturated)**

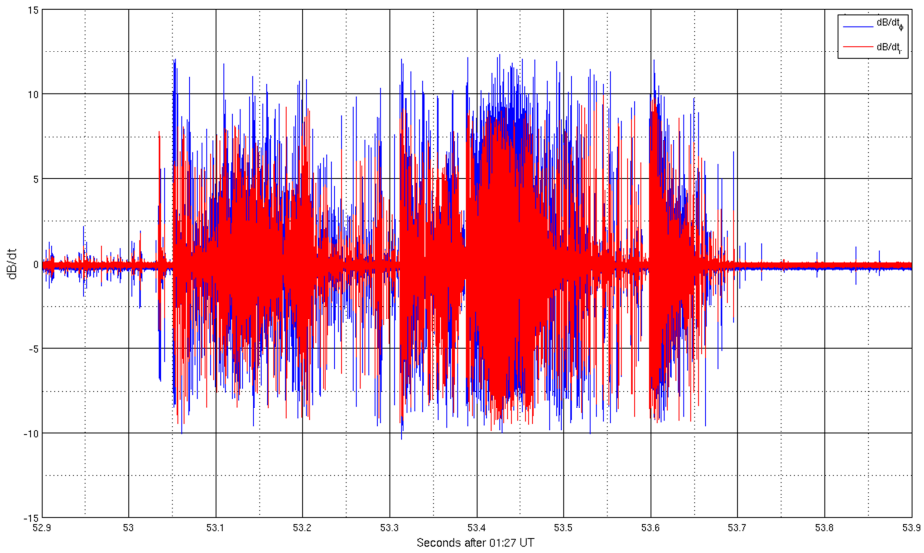


**Figure 44: Corresponding LF plot which is remarkably similar to VHF**

# 6. Useful frequency bands at Duke Campus

By looking at United States frequency allocation of radio spectrum, the choice of UHF band was quite obvious. A radio astronomy band at 608-614 MHz was perfect, as no one is allowed to transmit in that frequency band except land mobile (medical telemetry). Therefore, the recordings at Duke Campus at clear day (no thunderstorms) displayed least noise in that frequency band. Unfortunately, the choice of VHF band wasn't that easy. Following is the procedure employed to figure out less noisy VHF band.

With TVRX2 daughterboard and USRP N210, measurements were taken starting from 60MHz to 200MHz frequency with 10MHz of bandwidth and 16 dB gain. The recorded data was then analyzed on MATLAB at both time and frequency domain. Threshold calculations were done to the entire recorded data files (3 min each file, e.g. 60-70 MHz) to check less frequent radiation. The saturation range of the USRP was known (-0.3 to 0.3), although not calibrated in terms of units (in both, time and frequency domain). From the spectrogram (complex baseband), noise level in the different frequency bands was checked. If 5-6 MHz of the 10MHz recorded bandwidth seemed less noisy, then that frequency band was streamed again to verify the noise level. After doing this process several times, following were the selected frequency bands. Noise level increases as the index increases (e.g. number 8 has the highest noise level amongst all)

1. 73-74 MHz, Radio astronomy
2. 190-198 MHz, Broadcasting (TV channels 7-13)
3. 144-148 MHz, Amateur, amateur-satellite band
4. 170-180 MHz, Mobile, land mobile & broadcasting (TV channels 7-13)
5. 74-80MHz, Mobile, aeronautical radio navigation, broadcasting (TV channels 5-6)
6. 80-88 MHz, Broadcasting (TV channels 5-6)
7. 67-70 MHz, Broadcasting (TV channels 2-4)
8. 130-140 MHz, Aeronautical mobile, mobile, space-research (space to earth), mobile-satellite (space to earth)

154-158 MHz (land mobile, maritime mobile, mobile except aeronautical mobile) band was almost as good as Radio astronomy band. However, occasionally, signals with significant amplitude were detected, lasting for few seconds.

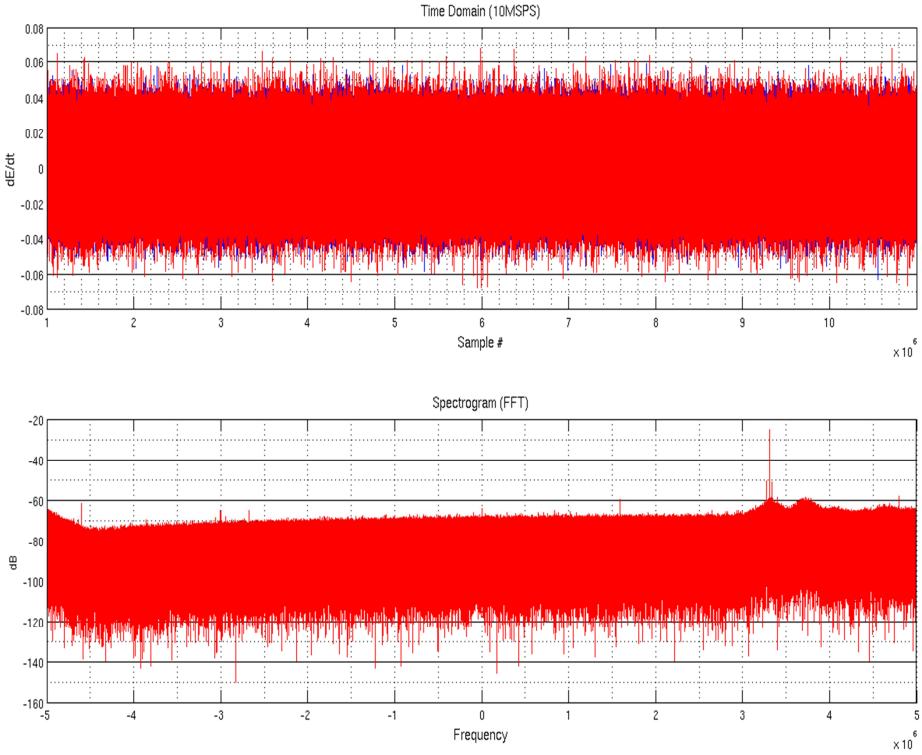


**Figure 45: Recorded at 190-200 MHz, from the spectrograph (195MHz is center frequency shown as 0 in the plot, indicating complex baseband signal), 190-198 MHz is less noisy in frequency domain**

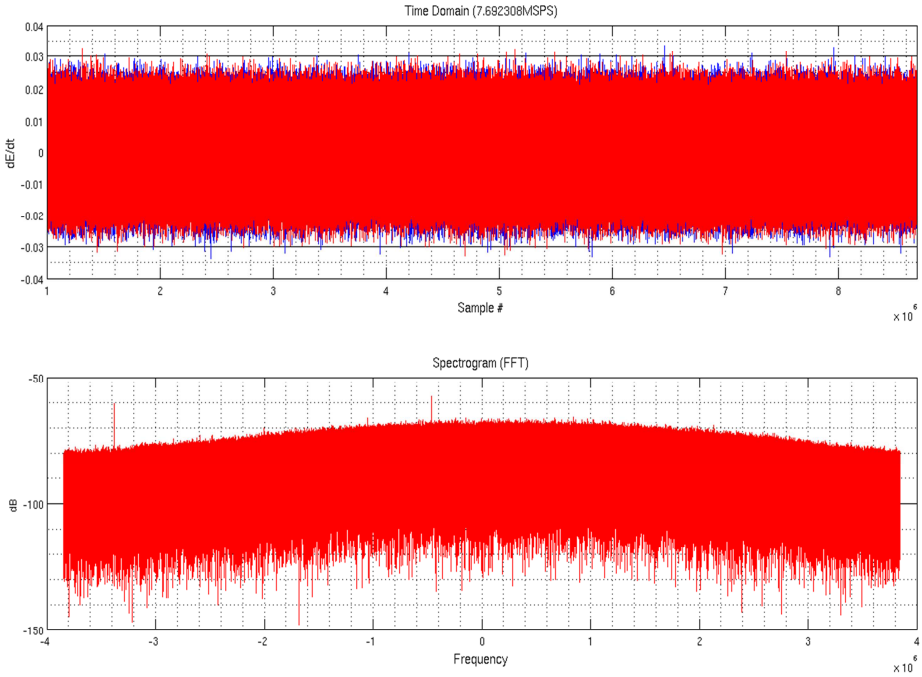


**Figure 46: Recorded with 194 MHz center frequency and 7.692308MHz bandwidth, showing less noise in time and frequency domain as expected**

# 7. Measurements at Duke Campus

Since the frequency bands were changed, evaluation of system was necessary (e.g. IC or CG detection range). The number of flashes observed were around 300 so instead of geometric location plots, the magnitude distance comparison is presented.

## *7.1 VHF (190-198 MHz)*

As noted previously, the time window (around NLDN UTC time) during which the maximum field change is represented is minimum of {1 second, $\frac{d_{i-1}}{d_i + d_{i-1}} t_1 + \frac{d_{i+1}}{d_i + d_{i+1}} t_2$ } where $t_1 = (t_i - t_{i-1})$ and $t_2 = (t_{i+1} - t_i)$ is time (seconds) between two NLDN events, while $d_i$ is the distance of $i^{th}$ event from Duke Campus. (NLDN time window is defined as 0.1 milliseconds here) For deciding whether particular flash is detected or not, the absolute value of $\frac{\partial E}{\partial t}$ during NLDN time window was compared with a threshold value (depending upon noise level). If the $|\frac{\partial E}{\partial t}|$ > threshold, then the flash is detected. However, from previous examples of CG, VHF was usually not significant during return strokes (NLDN generally reports time of first return stroke) and maximum outside NLDN time window. Therefore, the maximum $|\frac{\partial E}{\partial t}|$ was calculated in entire time window (less than 1 second) calculated previously.

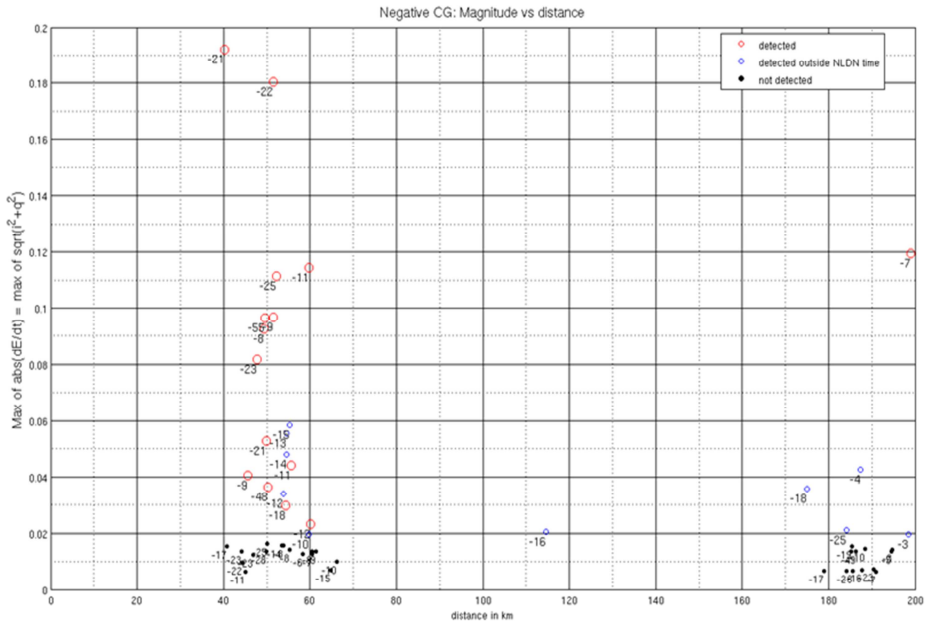


**Figure 47: For negative CG**

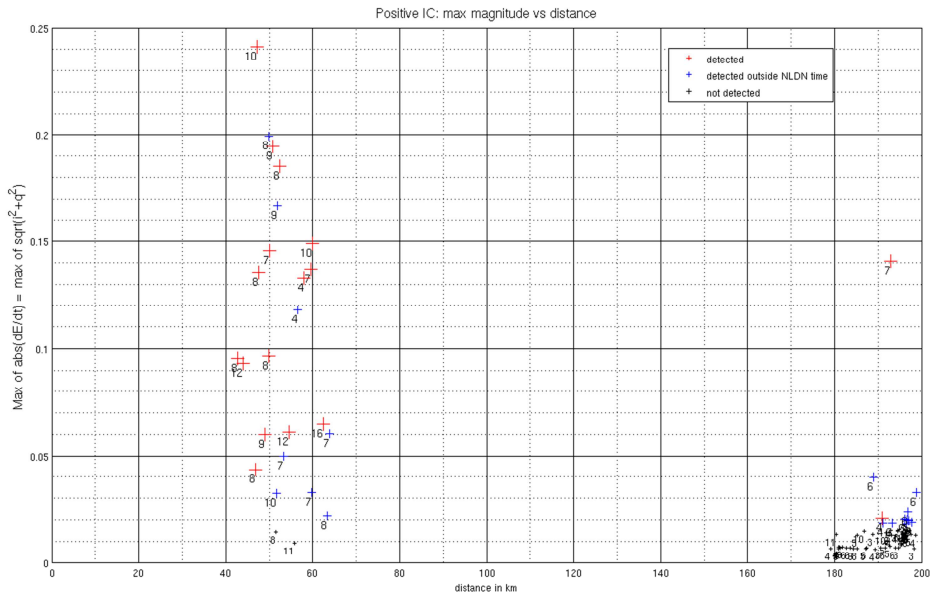


**Figure 48: For positive IC**

## *7.2 UHF (608-614 MHz)*

For UHF plots only 0.1 milliseconds of time duration was taken into consideration, as UHF had pulse sequences only for close flashes.

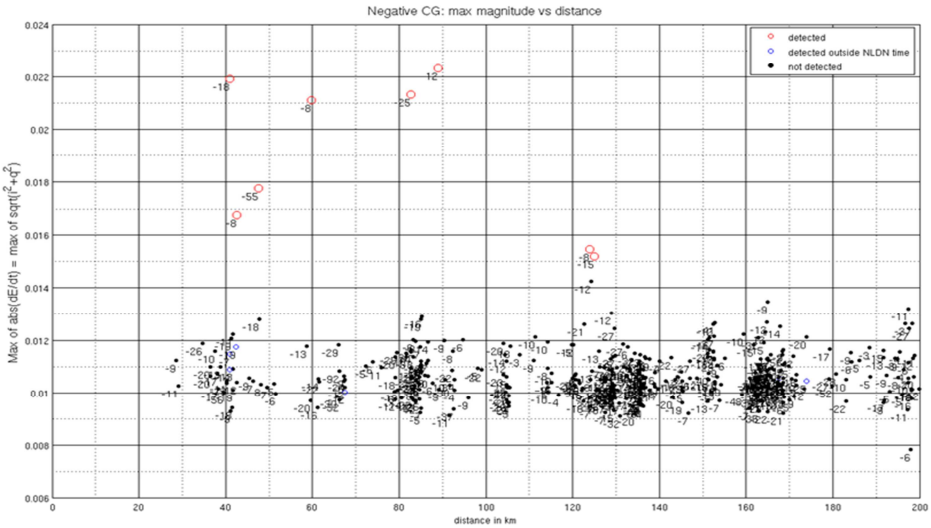


**Figure 49: Maximum of $|\frac{\partial E}{\partial t}|$ in 0.1 millisecond time window for negative CG**

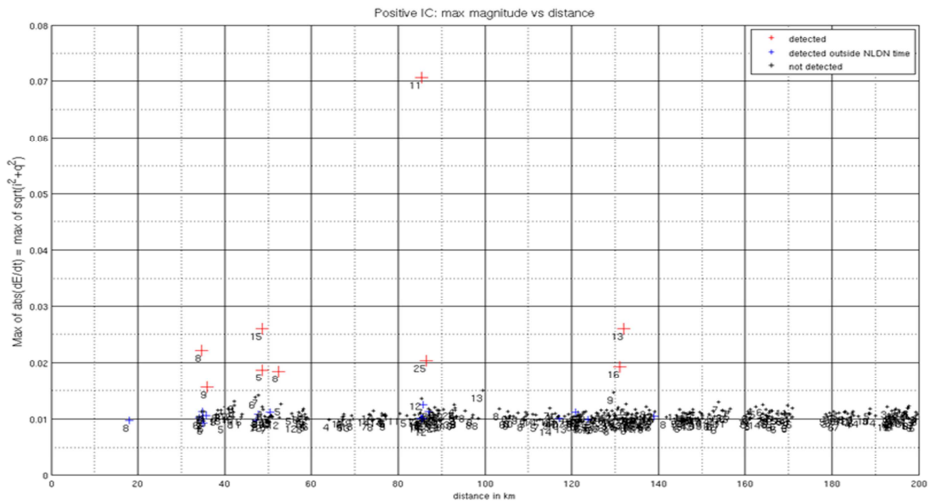


**Figure 50: For positive IC**

## *7.3 Inference of simultaneous UHF-VHF-LF recording*

In this section, the results are shown via specific plot in Figure 51 (UHF 608.5-613.5 MHz, VHF 191.5-196.5 MHz) but the similar results were observed in other flashes. Initial breakdown in cloud discharges is clearly visible at VHF and LF but not significant at UHF. Instead, UHF radiation is strong at probably stepped leaders, as the time duration of such pulses is only 1 to 2.5 μs (same duration at VHF). Such leaders are visible at LF but with extremely small magnitude. K processes or regular pulse bursts are clearly visible at UHF-VHF-LF making them broadband radiators, although small magnitude observed at UHF. In the plot below, four K processes were observed before the last IC. Most probably last IC turned to CG (but not reported by NLDN), as a first return stroke can be observed in Figure 53, again peak of the return stroke clearly invisible at VHF-UHF. Two subsequent return strokes were observed later in time. Regular pulse bursts associated with this CG were observed in between return stokes at UHF-VHF-LF, one example is Figure 54. The highest magnitude UHF event in Figure 52, occurring much before the CG, had different magnitude in each frequency band. The same figure displayed probably a leader activity at VHF, before and after the high magnitude event. The process in Figure 55 is not identified but was not observed in many IC (Since the event is much before the time of CG, it is clearly associated with IC). Interestingly, during this process LF was saturated but VHF-UHF radiation was not significant at all. Another process worth reporting is Figure 56. Interestingly, the high

magnitude pulses were saturated in all frequency bands and having similar magnitudes.

At VHF, may be a leader type of process is preceding higher magnitude pulses.

**Table 1: The flashes reported by NLDN, occurred during the time window of Figure 51**

| UTC time | Distance (km) | Current (kA) | CG=0 or IC=1 |
|---|---|---|---|
| 23:24:31.032 | 12.5471 | 10 | 1 |
| 23:24:31.034 | 12.016 | 8 | 1 |
| 23:24:31.04 | 12.6936 | 7 | 1 |
| 23:24:31.051 | 12.2414 | 6 | 1 |
| 23:24:31.453 | 15.18 | 6 | 1 |

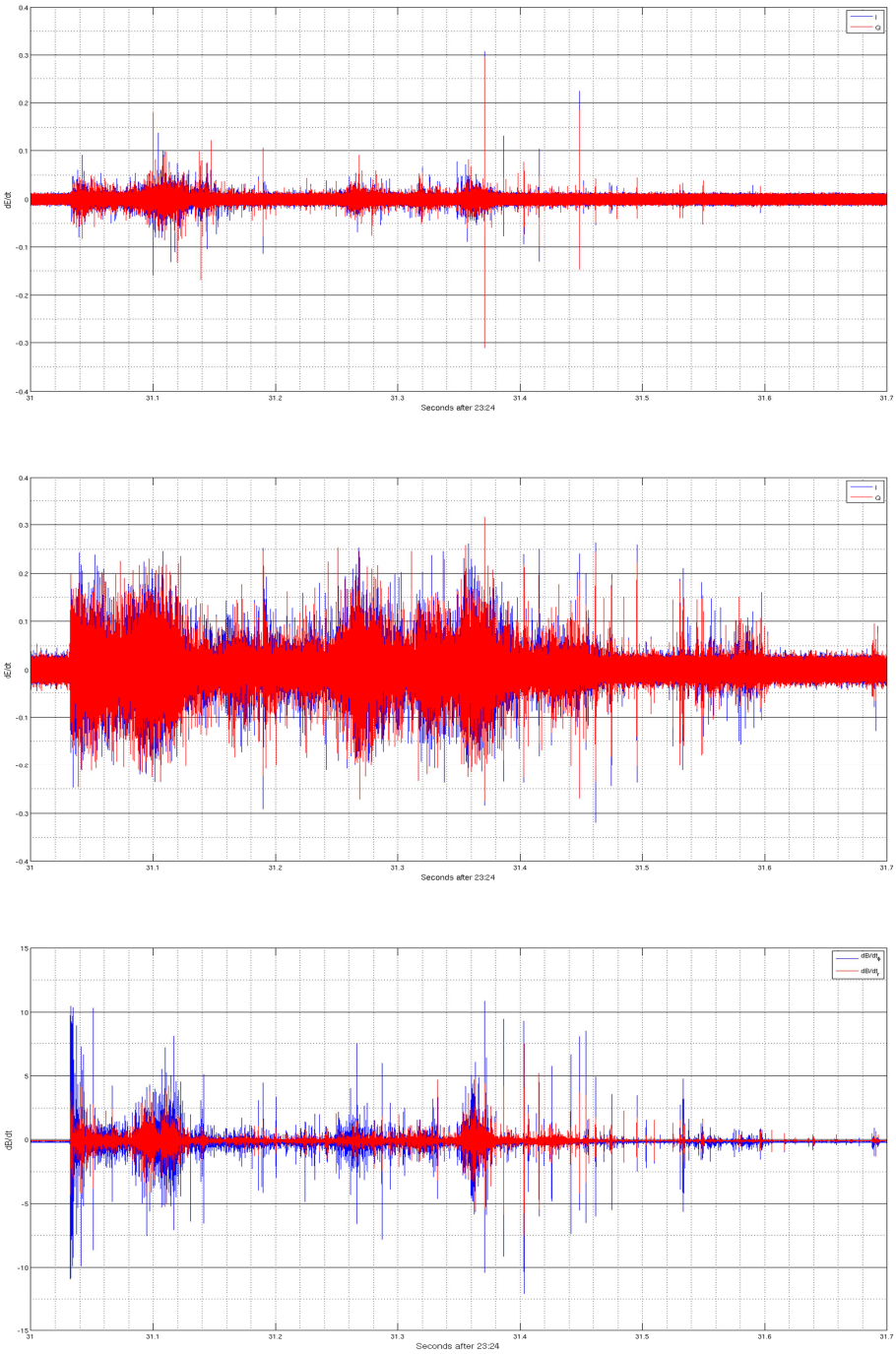


Figure 51: From top UHF, VHF and LF plots for flashes in Table 1

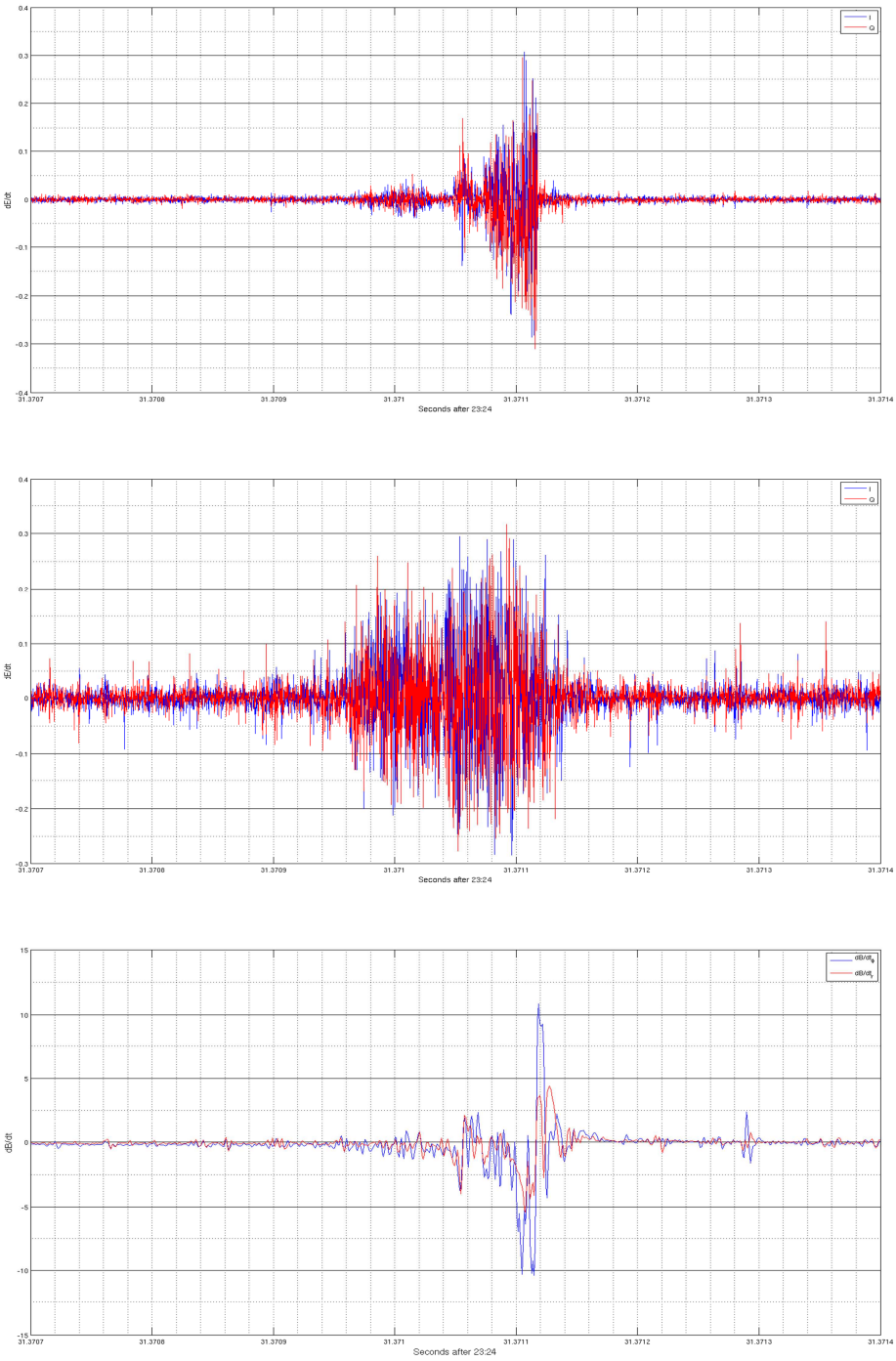


**Figure 52: Highest magnitude event at UHF**

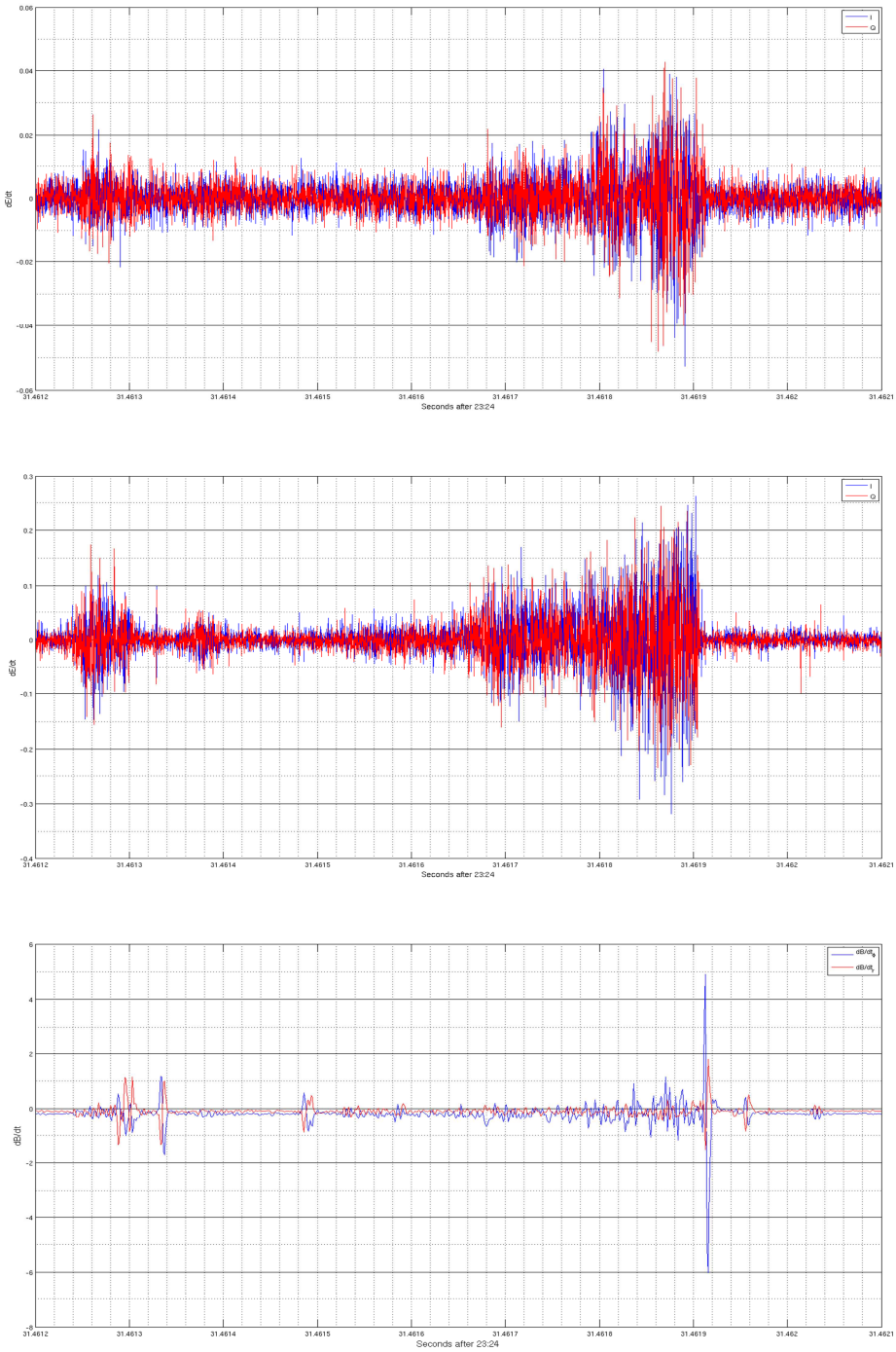


**Figure 53: Return stroke most probably**

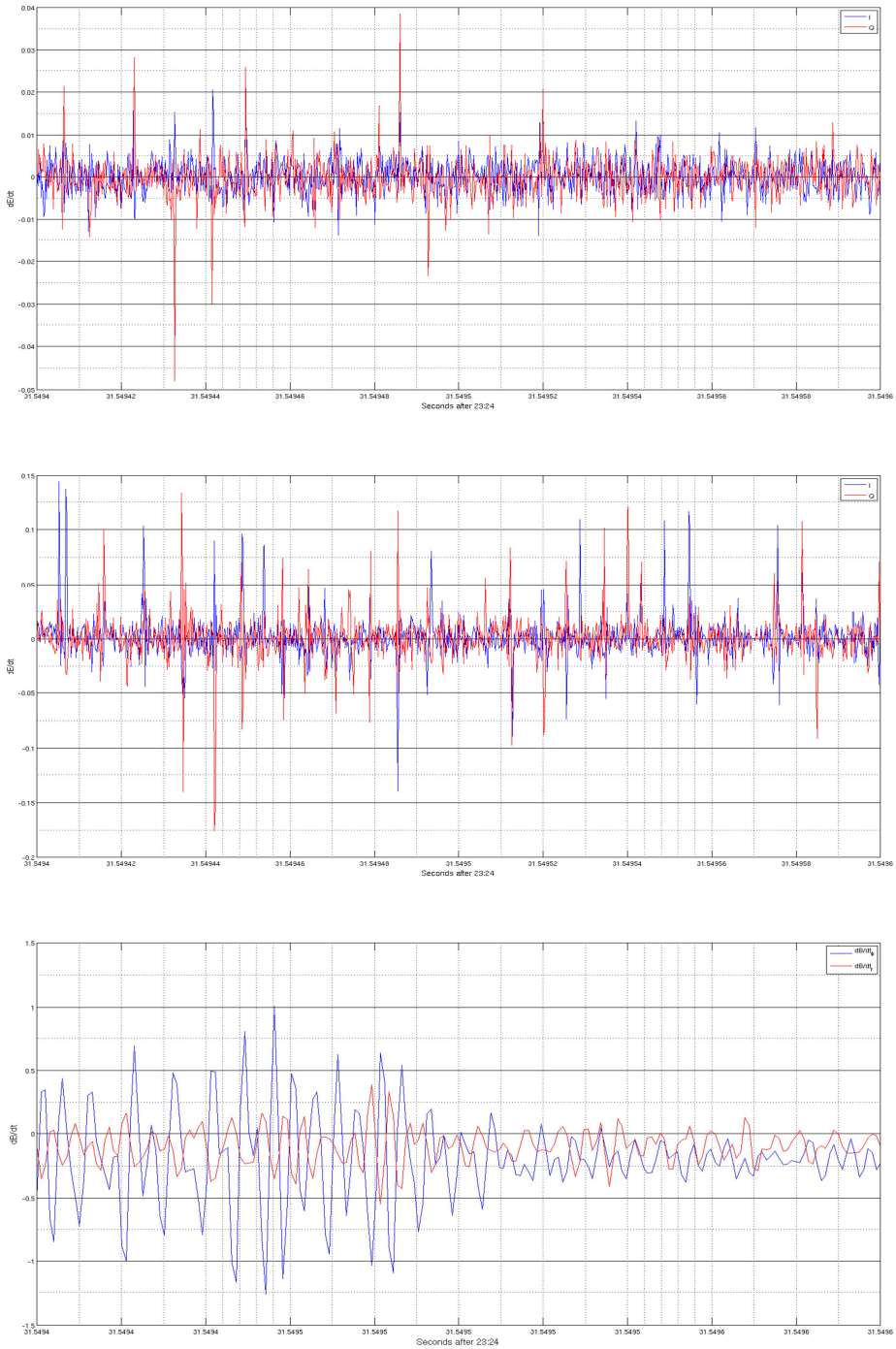


**Figure 54: Regular pulse burst**

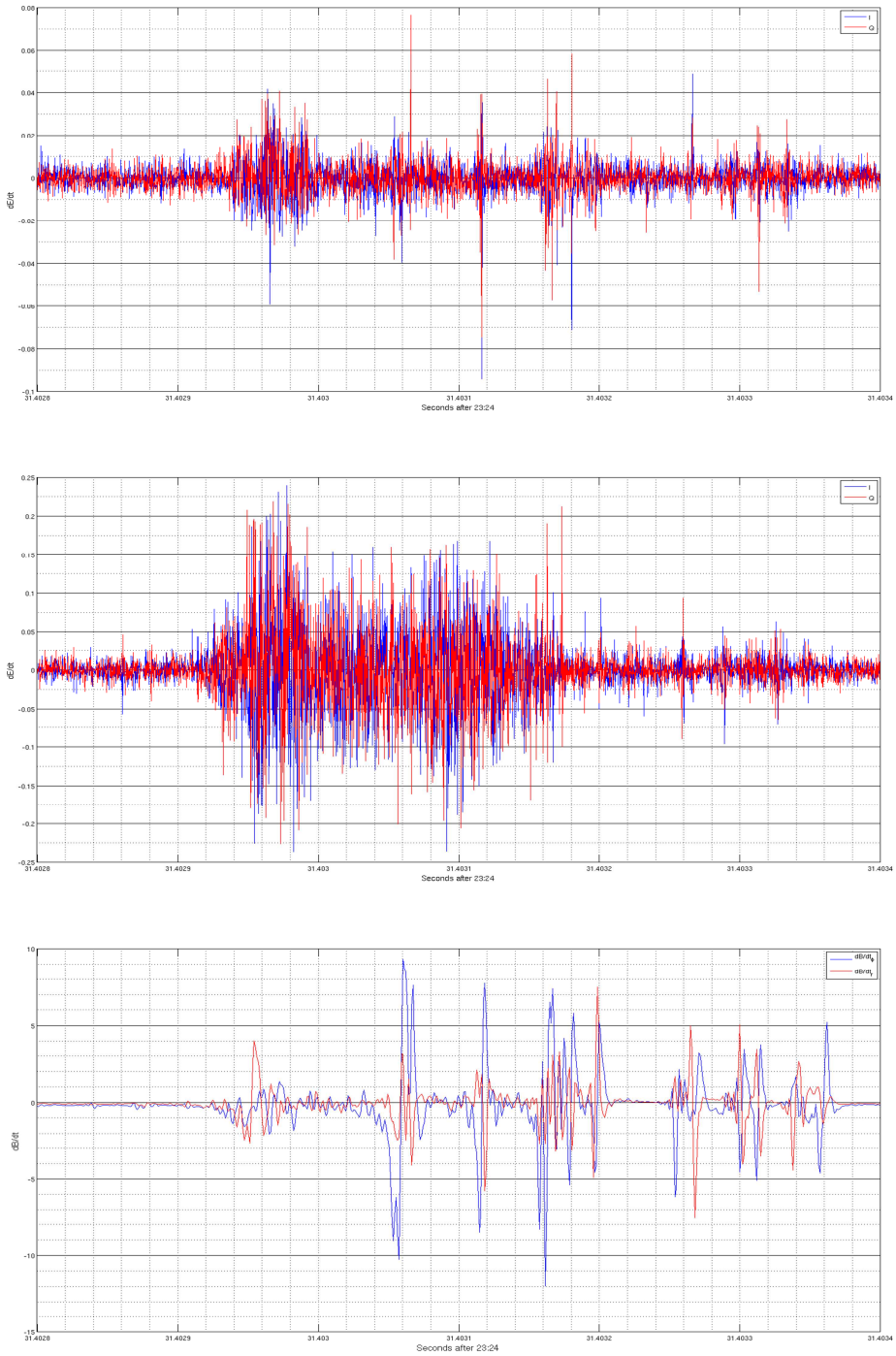


**Figure 55: Event of uncertain origin**

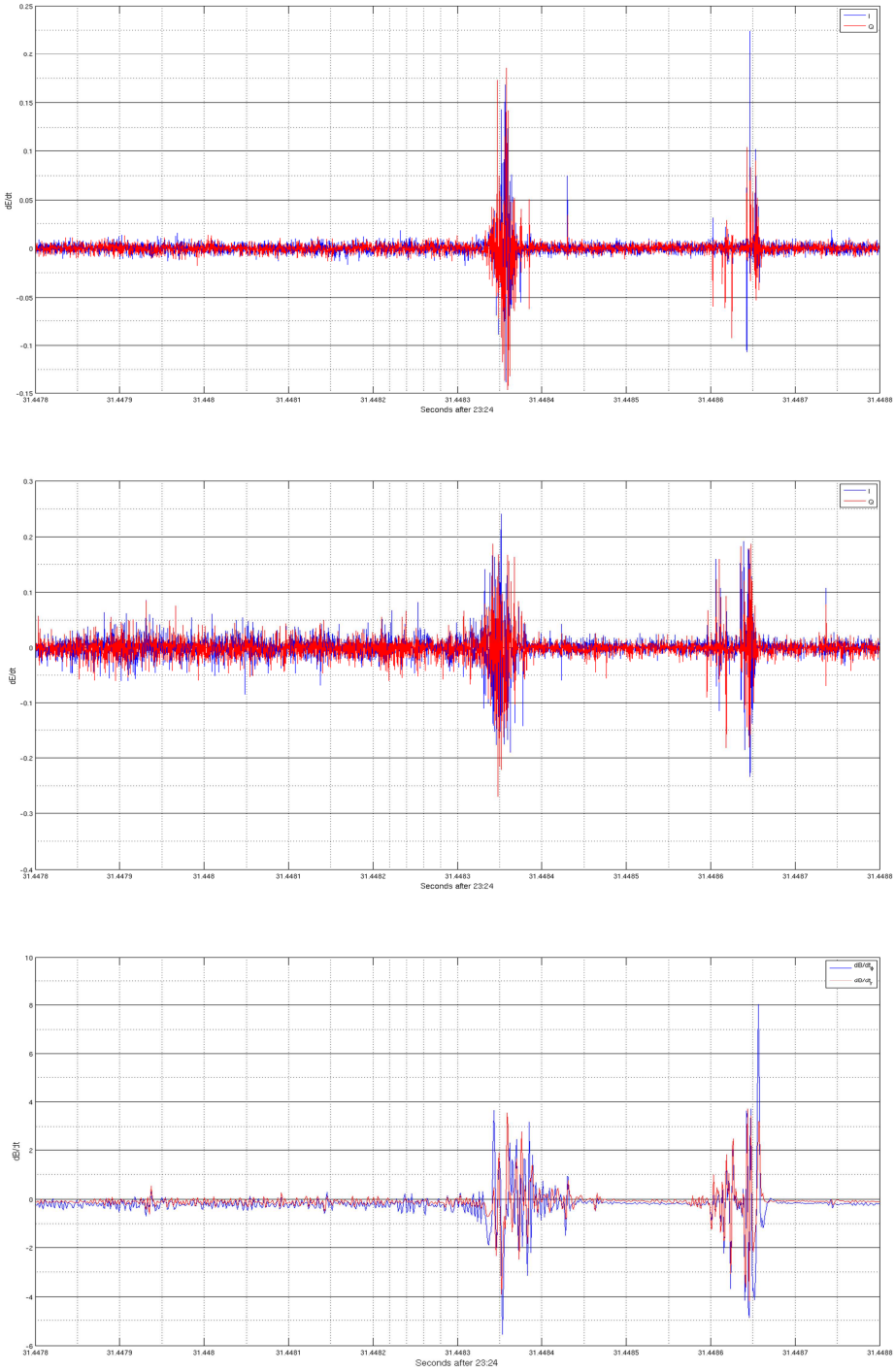


**Figure 56: Another event of uncertain origin**

# References


Davis, S. M. (1999). Properties of lightning discharges from multiple-station wideband electric field measurements.

Feynman, R. P., et al. (1964). "The Feynman lectures on physics." Physics Today **17**: 45.

Krehbiel, P. R., et al. (1979). "An Analysis of the Charge Structure of Lightning Discharges to Ground." J. Geophys. Res. **84**(C5): 2432-2456.

Lathi, B. P. (1998). Modern Digital and Analog Communication Systems 3e Osece, Oxford university press.

Le Vine, D. M. (1980). "Sources of the Strongest RF Radiation From Lightning." J. Geophys. Res. **85**(C7): 4091-4095.

Mahapatra, P., et al. (1999). Aviation Weather Surveillance Systems: Advanced Radar and Surface Sensors for Flight Safety and Air Traffic Management, Inst of Engineering & Technology.

Proctor, D. E. (1981). "VHF Radio Pictures of Cloud Flashes." J. Geophys. Res. **86**(C5): 4041-4071.

Proctor, D. E. (1997). "Lightning flashes with high origins." J. Geophys. Res. **102**(D2): 1693-1706.

Rakov, V. A. and M. A. Uman (2003). Lightning: physics and effects, Cambridge University Press.

Shao, X. M. and P. R. Krehbiel (1996). "The spatial and temporal development of intracloud lightning." J. Geophys. Res. **101**(D21): 26641-26668.

Williams, E. R. (1989). "The Tripole Structure of Thunderstorms." J. Geophys. Res. **94**(D11): 13151-13167.